Identification and functional characterization of a conserved sea snake cathelicidin SS-CATH against multidrug-resistant Gram-negative bacteria

Mei-Lin Xu[1,4,#], Shuang-Yu Li[1,4,#], Zhi-Kang Xu[2], Zhi-Zhen Liu[1,3], Yi-Xiao Song[1,4], Jing-Jing Zhang[1,4], Xiang-Jin Kong[1,4], Peng Song[5,6,*], Yi-Peng Wang[1,4,*]

[1]Yantai Institute of Coastal Zone Research, Chinese Academy of Sciences, Yantai, Shandong 264003, China

[2]Jiangsu Key Laboratory for the Biodiversity Conservation and Sustainable Utilization in the Middle and Lower Reaches of Yangtze River Basin, College of Life Sciences, Nanjing Normal University, Nanjing, Jiangsu 210000, China

[3]School of Biological Science and Technology, University of Jinan, Jinan, Shandong 250022, China

[4]University of Chinese Academy of Sciences, Beijing 100049, China

[5]School of Pharmaceutical Sciences and Food Engineering, Liaocheng University, Liaocheng, Shandong 252000, China

[6]State Key Laboratory of Macromolecular Drugs and Large-Scale Preparation, Liaocheng, Shandong 252000, China

[#]These authors contributed equally.

*Corresponding author: P.S. (email: songpeng@lcu.edu.cn); Y.P.W. (email: ypwang@yic.ac.cn).

Uncorrected proof

ABSTRACT

Sea snakes are fully marine-adapted reptiles living under unique environmental pressures, including high salinity and exposure to potentially pathogenic Gram-negative bacteria. Cathelicidin antimicrobial peptides (AMPs) are important components of vertebrate innate immunity, and their mature peptide sequences are typically highly diverse among species. Here, genome mining and comparative sequence analysis across multiple sea snake species were performed and an unusually conserved mature cathelicidin peptide, designated SS-CATH, was identified from the sea snake species of *Hydrophis cyanocinctus*, *Hydrophis major*, *Hydrophis elegans*, and *Hydrophis ornatus*. Functional characterization demonstrated that SS-CATH possesses potent and broad-spectrum bactericidal activity against multidrug-resistant (MDR) Gram-negative pathogens. Moreover, SS-CATH effectively inhibits biofilm formation, eradicates pre-established biofilms, and eliminates rifampicin-induced persisters. Mechanistic studies demonstrated that SS-CATH disrupted bacterial membranes and induced oxidative stress. SS-CATH also exhibited DNA-binding activity *in vitro*. In a murine peritonitis model, SS-CATH significantly improved host survival and reduced bacterial loads across multiple organs. The sequence conservation of SS-CATH suggests possible functional constraint, while its antibacterial activities highlight its potential role in host defense. These findings suggest SS-CATH as a promising therapeutic candidate against MDR Gram-negative infections and provide novel insights into innate immune adaptation in marine reptiles.

Keywords: Sea snake; Cathelicidin; Antimicrobial peptide; Extended-spectrum β-lactamase (ESBL)-producing *Escherichia coli*; Sequence conservation

Uncorrected proof

INTRODUCTION

Sea snakes (*Hydrophiinae*) are a lineage of reptiles that has fully adapted to marine habitats. They returned to the ocean from terrestrial elapid ancestors approximately 15 Ma. This evolutionary transition exposed them to strong selective pressures imposed by extreme environmental changes, including osmotic adaptation to high salinity, deep-sea hydrostatic pressure, and dramatic shifts in pathogen composition (Li et al., 2021; Ludington et al., 2023). Unlike terrestrial and freshwater snakes, the skin and mucosal surfaces of sea snakes are continuously exposed to a marine environment with a high microbial load. Microbiome studies of *Hydrophis cyanocinctus* and *Hydrophis curtus* have revealed a high abundance of Gram-negative taxa in the gut, particularly members of Proteobacteria and Enterobacteriaceae. Several Gram-negative genera, including *Arcobacter*, *Pseudomonas*, *Tenacibaculum*, and *Vibrio*, have also been detected in their skin microbiota, particularly in association with skin ulceration (Zhong et al., 2022, 2023). As several of these taxa include opportunistic pathogens, exposure to Gram-negative bacteria may constitute an important microbial challenge to sea snakes, particularly when epithelial barriers are compromised. This long-term host–pathogen coexistence has imposed substantial evolutionary pressure on the sea snake innate immune system, driving the emergence of highly efficient and specialized antimicrobial effectors that maintain epithelial barrier integrity and microbial homeostasis (Li et al., 2021).

Cathelicidin family antimicrobial peptides (AMPs) are key effector molecules of the vertebrate innate immune system (Bucataru & Ciobanasu, 2024). They are widely distributed in mammals, birds, amphibians, fishes, and reptiles, where they play essential roles in early host defense (Mhlongo et al., 2023; Yadav & Chauhan, 2024). Cathelicidin precursor peptides consist of an N-terminal signal peptide, a conserved cathelin domain, and a highly variable C-terminal mature peptide region (Chai et al., 2021). The cathelin domain exhibits remarkable sequence conservation across species, providing a reliable molecular marker for the

uncorrected proof

identification of novel cathelicidins (Bals & Wilson, 2003; Salnikov et al., 2025). In contrast, the mature peptide region displays substantial diversity in amino acid composition, peptide length, charge distribution, and hydrophobicity. These variations largely determine the antimicrobial spectrum (Xuan et al., 2023), bactericidal mechanisms, and target selectivity of cathelicidins from different species (Tajer et al., 2024). Most mature cathelicidin peptides are cationic and initially target the negatively charged bacterial membrane through electrostatic interactions. Some members can further penetrate the membrane and interact with intracellular targets, including DNA, RNA, or essential enzymes, thereby exerting multitarget antibacterial activity. This mode of action contributes to the broad-spectrum antimicrobial activity of cathelicidins while reducing the likelihood of resistance development (Mhlongo et al., 2023; Yadav & Chauhan, 2024).

In recent years, cathelicidin AMPs have attracted growing scientific interest. However, research on these peptides derived from sea snakes remains in its infancy. In 2015, our group reported the first identification of cathelicidin AMP (Hc-CATH) from sea snake (*H. cyanocinctus*). Hc-CATH exhibited both antimicrobial and anti-inflammatory activities *in vitro* and *in vivo*, and significantly reduced bacterial burdens in a murine lung infection model (Wei et al., 2015). Subsequently, Wang et al. (2023) identified Hydrostatin-AMP2, another cathelicidin, from the same species. More recently, Pan et al. (2025a) identified Hydrostatin-AMP3 from *H. curtus* through a genome-mining strategy. To date, only three cathelicidin peptides have been isolated and comprehensively characterized from sea snakes (Gao et al., 2025). Critically, all existing studies have focused either on single species or on individual peptides, with no cross-species or phylogenetically informed analyses conducted. Consequently, a systematic understanding of the evolutionary dynamics, structural diversification, and potential ecological roles of cathelicidins across sea snake genera remains absent.

Uncorrected proof

In this study, we conducted the first systematic genome mining of cathelicidins in the sea snake subfamily Hydrophiinae. Unexpectedly, we identified a cathelicidin peptide, designated SS-CATH, whose mature peptide sequence is not only completely identical but also remarkably conserved across multiple sea snake species. This finding sharply contrasts with the prevailing view that cathelicidin mature peptides are structurally highly diverse. Even within a single species, different cathelicidins often exhibit substantial sequence variation and minimal similarity (Bals & Wilson, 2003; Peel et al., 2025). Functional characterization demonstrated that SS-CATH exhibited potent antibacterial activity against multidrug-resistant (MDR) Gram-negative pathogens. Mechanistic studies demonstrated membrane disruption and oxidative stress induction by SS-CATH. The peptide also exhibited DNA-binding activity *in vitro*. In addition, SS-CATH displayed potent antibiofilm and anti-persister activities, favorable stability, acceptable *in vitro* biocompatibility, and significant therapeutic efficacy in a murine peritonitis model. These findings identify SS-CATH as a conserved AMP with potent antibacterial activity and provide a basis for exploring the evolution of innate immunity in marine reptiles.

MATERIALS AND METHODS

Identification and sequence analysis of SS-CATH

Annotated snake cathelicidin precursor protein sequences were retrieved from the National Center for Biotechnology Information (NCBI) database and used as reference sequences. Multiple sequence alignment was performed to identify the highly conserved cathelin-like domain (CLD). The conserved CLD sequence was subsequently used as the query for TBLASTN searches against available sea snake genome assemblies to identify putative CATHL loci. For each positive hit, the flanking genomic regions (3 kb upstream and

uncorrected proof

downstream) were extracted, and gene structures were predicted using GeneWise. The optimal gene models were selected based on alignment scores and the characteristic four-exon organization of the cathelicidin family, followed by manual curation and validation according to the predicted mature peptide sequences.

A total of six cathelicidin precursor sequences were identified from five sea snake species, including *Aipysurus laevis* (AL-1, AL-2)*, H. cyanocinctus, Hydrophis major, Hydrophis elegans, and Hydrophis ornatus*. The mature peptide sequences of *H. cyanocinctus*, *H. major, H. elegans, and H. ornatus* were identical and exhibited remarkable sequence conservation. This conserved mature peptide was designated SS-CATH and selected for subsequent functional characterization.

Multiple sequence alignment was performed using Molecular Evolutionary Genetics Analysis (MEGA). Signal peptides and cleavage sites were predicted using SignalP v.6.0. Functional regions, including the signal peptide, cathelin-like domain, and mature peptide, were annotated based on the conserved cysteine residues characteristic of the cathelicidin family. The three-dimensional structure of the mature peptide was predicted using AlphaFold3, and the helical wheel projection was generated using HeliQuest with the complete 34-amino-acid sequence of mature SS-CATH to analyze its amphipathic α-helical structure and the spatial distribution of hydrophobic and hydrophilic residues. Physicochemical properties, including molecular weight (MW), theoretical isoelectric point (pI), net charge at physiological pH, and the grand average of hydropathicity (GRAVY), were calculated using the ExPASy ProtParam server.

Peptide synthesis

The SS-CATH peptide (KRFKKFFKKLKESVKKRVKEFFKKPTVIGVSIPF) was synthesized by GL Biochem (China) using the solid-phase peptide synthesis method. Peptide

Uncorrected proof

purity (>95%) was confirmed by reversed-phase high-performance liquid chromatography (RP-HPLC), and the peptide sequence was verified by electrospray ionization mass spectrometry (ESI-MS).

Circular dichroism (CD) analysis

The secondary structural characteristics of the peptides were analyzed by CD spectroscopy according to the method described in reference (Zhang et al., 2022). The peptides were dissolved separately in distilled water and 60 mmol/L sodium dodecyl sulfate (SDS) solution, and the final concentration was adjusted to 0.2 mg/mL. CD spectra were recorded from 190 to 260 nm at 298 K using a Chirascan circular dichroism spectrometer (Applied Photophysics, UK). The measurement parameters were set as follows: path length, 0.1 cm; bandwidth, 1 nm; response time, 1 s; scanning speed, 100 nm/min.

Bacterial strains

The reference bacterial strains used in this study were obtained from our laboratory collection, including *Escherichia coli* ATCC25922, *Klebsiella pneumoniae* ATCC10031, *Acinetobacter baumannii* ATCC19606, *Staphylococcus aureus* CMCC26003, *Aeromonas hydrophila*, *Edwardsiella tarda*, *Bacillus cereus* CMCC63301, Methicillin-resistant *Staphylococcus aureus* (MRSA) 52, and Methicillin-resistant *Staphylococcus aureus* USA300.

Clinical isolates were obtained from the existing bacterial culture collection of the First People's Hospital of Zunyi and their collection was approved by the Ethics Committee of the Yantai Institute of Coastal Zone Research, Chinese Academy of Sciences. These isolates included extended-spectrum β-lactamase (ESBL)-producing *Escherichia coli* 1, ESBL-producing *Escherichia coli* 2, ESBL-producing *Escherichia coli* 3, ESBL-producing

uncorrected proof

Escherichia coli 4, MDR *Acinetobacter baumannii* 1, MDR *Acinetobacter baumannii* 2, MDR *Acinetobacter baumannii* 3, Carbapenem-resistant (CR) *Klebsiella pneumoniae* 1, CR *Klebsiella pneumoniae* 3, MDR *Pseudomonas aeruginosa* 1, MDR *Pseudomonas aeruginosa* 2, MDR *Pseudomonas aeruginosa* 3, MDR *Staphylococcus aureus* 2, MDR *Staphylococcus aureus* 3, MDR *Staphylococcus epidermidis* 1, MDR *Staphylococcus epidermidis* 2, and MDR *Staphylococcus epidermidis* 3.

Species identification was performed using the VITEK 2 system. Antimicrobial susceptibility was assessed by minimum inhibitory concentration (MIC) determination and disk diffusion testing, and the results were interpreted according to Clinical and Laboratory Standards Institute (CLSI) M100, 33rd edition. ESBL-producing isolates were identified by antimicrobial susceptibility testing combined with polymerase chain reaction (PCR)-based molecular detection. Multidrug resistance was defined as acquired non-susceptibility to at least one agent in three or more antimicrobial categories (Magiorakos et al., 2012). Carbapenem-resistant *K. pneumoniae* isolates were classified based on resistance to imipenem and/or meropenem according to the applicable CLSI breakpoints.

All bacterial strains were stored and cultured under biosafety-compliant laboratory conditions.

MIC assay

The *in vitro* antibacterial activity of SS-CATH was evaluated using a modified broth microdilution method as previously described (Giacometti et al., 2000). Briefly, the peptide was serially two-fold diluted in a 96-well microtiter plate to obtain a range of concentrations. Bacterial cultures were grown to the mid-logarithmic phase, and the cell density was adjusted to 2×10^5 colony-forming units (CFU)/mL in Mueller–Hinton (MH) broth. Equal volumes of the bacterial suspension were then added to each well and incubated at 37°C for 18 h. The MIC

uncorrected proof

was defined as the lowest peptide concentration that completely inhibited visible bacterial growth. For calculation of the geometric mean (GM) MIC, values reported as >100 μg/mL were assigned a value of 100 μg/mL. Accordingly, GMs calculated using these values represent lower-bound estimates. All experiments were performed in three independent biological replicates.

Bacterial growth curve assay

The inhibitory effect of SS-CATH on the growth of ESBL-producing *E. coli 4* was evaluated by monitoring bacterial growth over 18 h. Fresh bacterial colonies were inoculated into MH broth and cultured to the logarithmic phase, then diluted with fresh MH broth to 1×10^6 CFU/mL. The bacterial suspension was added to sterile 96-well plates, followed by SS-CATH at final concentrations of 0.5×, 1×, 2×, and 5×MIC. Polymyxin B (Solarbio, China) at 5×MIC served as the positive control, and phosphate-buffered saline (PBS; Aladdin, China) served as the negative control. Optical density (OD) at 600 nm was measured every 30 min at 37°C over 18 h using a microbial growth curve analyzer (Scientz, China), and growth curves were plotted.

Time–kill kinetics assay

The bactericidal kinetics of SS-CATH were evaluated using a time–kill assay as previously described (Kavela et al., 2025). Briefly, ESBL-producing *E. coli* 4 cultures in the mid-logarithmic growth phase were diluted to 1×10^6 CFU/mL in fresh medium and mixed with equal volumes of SS-CATH at the indicated concentrations or the positive control antibiotic. The mixtures were incubated at 37°C, and samples were collected at the designated time points. Each sample was serially diluted, spread onto Luria–Bertani (LB) agar plates (Hopebiol, China), and plated in triplicate. After incubation at 37°C for 18 h, the number of viable bacteria was determined by counting CFUs. All experiments were performed in three independent

Uncorrected proof

biological replicates.

Live/dead bacterial staining assay

Live/dead bacteria were assessed using SYTO-9 and propidium iodide (PI) staining (Li et al., 2026a). Mid-log-phase ESBL-producing *E. coli* 4 (1×10^8 CFU/mL) were treated with SS-CATH at indicated concentrations for 1 h at 37°C. Cells were harvested, washed twice with PBS, and stained with SYTO-9 (4 μmol/L) (Thermo Fisher Scientific, USA) and PI (15 μmol/L) (Sigma-Aldrich, USA) for 1 h at 37°C in the dark. Fluorescence images were acquired using a fluorescence microscope. One image covering a fixed field of view was acquired from each of three independent biological replicates per group. Representative images were randomly selected from the three images per group, and all three images were included in the quantitative analysis. Green and red fluorescence indicated live and dead bacteria, respectively. Images were quantified using ImageJ. SYTO-9 and PI fluorescence signals were quantified using the same image-analysis procedure for all groups. The relative proportions of live and dead fluorescence were calculated based on the SYTO-9 and PI fluorescence signals, respectively, with the total fluorescence signal normalized to 100%.

Assessment of resistance development

The potential of SS-CATH to induce ESBL-producing *E. coli* 4 resistance was evaluated using a serial passage assay. ESBL-producing *E. coli* 4 was selected as a clinically relevant resistant isolate and to maintain consistency with the strain used in the antibacterial activity and mechanistic assays. Mid-logarithmic-phase bacteria were inoculated into MH broth containing 0.5×MIC of the peptide and incubated at 37°C for 12 h, with each incubation representing one passage. This procedure was repeated for 40 consecutive passages. The MIC was determined every five passages to monitor changes in bacterial susceptibility during the

uncorrected proof

evolution of resistance.

Biofilm eradication assay

The biofilm eradication activity of SS-CATH against preformed ESBL-producing *E. coli* 4 biofilms was evaluated using crystal violet (CV) and 2,3,5-triphenyltetrazolium chloride (TTC) staining as previously described (Haney et al., 2018; Hanstein et al., 2025). Briefly, bacterial cultures in the mid-logarithmic growth phase were diluted to 1×10^7 CFU/mL in fresh medium, and 100 μL of the suspension was added to each well of a sterile 96-well plate. The plates were incubated statically at 37°C for 48 h to allow biofilm formation. After incubation, the culture supernatant was discarded, and the wells were gently washed with PBS to remove planktonic bacteria. Fresh medium containing SS-CATH at the indicated concentrations was then added, followed by incubation at 37°C for an additional 24 h.

For the CV assay, the supernatants were removed after peptide treatment, and the wells were washed twice with PBS. The remaining biofilms were fixed with methanol for 10 min, air-dried, and stained with 0.1% CV (Aladdin, China) for 20 min at room temperature in the dark. Excess stain was removed by washing with distilled water, and the plates were air-dried. The bound dye was dissolved in absolute ethanol, and absorbance was measured at 595 nm using a microplate reader (Tecan Group Ltd., Switzerland).

For the TTC assay, TTC (Aladdin, China) was added together with SS-CATH from a 0.5% stock solution to a final concentration of 0.05%. After the 24 h treatment period, the supernatants were removed, and the wells were washed twice with PBS. The TTC reduction product was dissolved in methanol, and absorbance was measured at 500 nm using a microplate reader (Tecan Group Ltd., Switzerland).

CV and TTC measurements were performed in separate parallel wells, with three independent biological replicates for each assay.

Uncorrected proof

Biofilm inhibition assay

The inhibitory effect of SS-CATH on ESBL-producing *E. coli* 4 biofilm formation was evaluated using CV and TTC staining as previously described (Haney et al., 2018; Hanstein et al., 2025). Briefly, ESBL-producing *E. coli* 4 cultures in the mid-logarithmic growth phase were diluted to 2×10^7 CFU/mL in fresh medium. Equal volumes of the bacterial suspension and SS-CATH at the indicated concentrations were mixed in sterile 96-well plates to achieve the same final volume in each well. The plates were then incubated statically at 37°C for 48 h to allow biofilm formation.

For the CV assay, the culture supernatants were discarded after incubation, and the wells were gently washed with PBS to remove non-adherent bacteria. The biofilms were fixed with methanol for 10 min, air-dried, and stained with 0.1% CV for 20 min at room temperature in the dark. Excess stain was removed by washing with PBS, and the plates were air-dried. The bound dye was dissolved in absolute ethanol, and absorbance was measured at 595 nm using a microplate reader (Tecan Group Ltd., Switzerland).

For the TTC assay, TTC was added together with SS-CATH at the beginning of incubation from a 0.5% stock solution to a final concentration of 0.05%. After the 48-h incubation period, the culture supernatants were discarded, and the wells were gently washed with PBS. The TTC reduction product was dissolved in methanol, and absorbance was measured at 500 nm using a microplate reader (Tecan Group Ltd., Switzerland).

CV and TTC measurements were performed in separate parallel wells, with three independent biological replicates for each assay.

Persister killing assay

The bactericidal activity of SS-CATH against bacterial persisters was evaluated using a

uncorrected proof

rifampicin-induced persister model as previously described, with modifications (Zhong et al., 2025). Briefly, ESBL-producing *E. coli* 4 cultures in the mid-logarithmic growth phase were diluted to 2×10^8 CFU/mL in fresh medium and treated with rifampicin (Aladdin, China) at 100×MIC for 24 h at 37°C. Following incubation, the supernatants were discarded, and the adherent bacterial cells were washed three times with PBS to remove non-adherent bacteria and residual rifampicin. The washed bacterial cells were then resuspended in PBS and disrupted by sonication to obtain a bacterial suspension. The resulting bacterial suspension was mixed with SS-CATH at the indicated final concentrations and incubated at 37°C for 12 h. After treatment, the cultures were serially diluted, spread onto LB agar plates, and incubated at 37°C for 18 h. Viable bacteria were quantified by counting CFUs. All experiments were performed in three independent biological replicates.

Stability assay

The effects of physiological ions and protease treatment on the antibacterial activity of SS-CATH were evaluated by determining the MIC using the broth microdilution method as previously described. For the ion stability assay, MH broth was supplemented individually with NaCl, KCl, $CaCl_2$, $FeCl_3$, $ZnCl_2$, or NH_4Cl (Aladdin, China) at final concentrations of 150 mmol/L, 4.5 mmol/L, 2 mmol/L, 4 μmol/L, 8 μmol/L, and 6 μmol/L, respectively, prior to MIC determination. Additional MIC measurements were performed at final NaCl concentrations of 100, 200, 300, 400, and 500 mmol/L to evaluate antibacterial activity under elevated NaCl conditions. For the protease stability assay, SS-CATH was dissolved in ultrapure water and incubated with trypsin, chymotrypsin or pepsin at 37°C for 2 h. Subsequently, the remaining antibacterial activity of treated peptide samples was evaluated via the standard MIC assay. All experiments were performed in three independent biological replicates.

Uncorrected proof

Hemolysis assay

The hemolytic activity of SS-CATH was evaluated using a mouse erythrocyte hemolysis assay. Fresh mouse erythrocytes were collected, washed with PBS, and mixed with equal volumes of SS-CATH at the indicated concentrations. After incubation at 37°C for 30 min, the samples were centrifuged at 1 200 r/min (centrifuge radius: 8 cm) for 5 min at 4°C, and the supernatants were collected. The absorbance was measured at 540 nm using a microplate reader (Tecan Group Ltd., Switzerland). Untreated erythrocytes suspended in PBS served as the negative control (0% hemolysis), whereas erythrocytes treated with 1% Triton X-100 (Aladdin, China) served as the positive control (100% hemolysis). The hemolysis rate was calculated by the following formula:

$$\text{Hemolysis rate (\%)}=\frac{\text{OD}_{540\text{ nm}}\text{ (peptides)}-\text{OD}_{540\text{ nm}}\text{ (PBS)}}{\text{OD}_{540\text{ nm}}\text{ (1\% Triton X-100)}-\text{OD}_{540\text{ nm}}\text{ (PBS)}}\times 100\%. \quad (1)$$

The experiments were performed in three independent biological replicates.

Cell viability assay

The *in vitro* cytotoxicity of SS-CATH was evaluated using the 3-(4,5-dimethylthiazol-2-yl)-2,5-diphenyltetrazolium bromide (MTT) assay as previously described (Ma et al., 2022). Human keratinocyte HaCat cells and murine macrophage RAW264.7 cells were cultured in Dulbecco's modified Eagle medium (DMEM; Thermo Fisher Scientific, USA) supplemented with 10% fetal bovine serum (FBS; Thermo Fisher Scientific, USA) at 37°C in a humidified incubator containing 5% CO_2. Cells were seeded into 96-well plates at a density of 2×10^4 cells/well in a final volume of 100 μL and incubated for 24 h to allow cell attachment. The culture medium was then replaced with fresh medium containing SS-CATH at the indicated concentrations. Wells containing cells without peptide treatment served as the negative control, while wells containing culture medium alone served as the blank control. After incubation for

Uncorrected proof

24 h, 20 μL of MTT solution (5 mg/mL; Sigma-Aldrich, USA) was added to each well, followed by incubation for 4 h at 37°C in the dark. The supernatant was carefully removed, and 150 μL of dimethyl sulfoxide (DMSO; Solarbio, China) was added to dissolve the formazan crystals. The absorbance was measured at 570 nm using a microplate reader (Tecan Group Ltd., Switzerland). Cell viability was calculated using the following equation:

$$\text{Inhibition rate (\%)} = \frac{\text{OD}_{570\,\text{nm}}\,\text{(drug)} - \text{OD}_{570\,\text{nm}}\,\text{(blank)}}{\text{OD}_{570\,\text{nm}}\,\text{(negative)} - \text{OD}_{570\,\text{nm}}\,\text{(blank)}} \times 100\%. \quad (2)$$

The experiments were performed in three independent biological replicates.

Membrane fluidity assay

Bacterial membrane fluidity was assessed using the fluorescent probe Laurdan (*Thermo Fisher Scientific*, USA) as previously described (Bessa et al., 2018). Briefly, mid-logarithmic-phase ESBL-producing *E. coli* 4 cultures were diluted to 1×10^8 CFU/mL in MH broth and incubated with 10 μmol/L Laurdan at 37°C for 30 min in the dark. After staining, SS-CATH was added at the indicated concentrations, and the samples were incubated for an additional 60 min in the dark. PBS and Triton X-100 were used as the negative and positive controls, respectively. Fluorescence was measured using an excitation wavelength of 350 nm and emission wavelengths of 440 nm and 490 nm. Membrane fluidity was quantified by calculating the generalized polarization (GP) value using the following equation:

$$\text{GP} = \frac{I_{440} - I_{490}}{I_{440} + I_{490}}. \quad (3)$$

Lipid-binding assay

The effects of exogenously added lipids on the antibacterial activity of SS-CATH were evaluated using a phospholipid inhibition assay based on the checkerboard broth microdilution method as previously described (Ye et al., 2024). Briefly, different concentrations of lipopolysaccharide (LPS) from *E. coli* O111:B4 and four phospholipids, including

uncorrected proof

phosphatidylglycerol (PG), phosphatidylethanolamine (PE), phosphatidylcholine (PC), and cardiolipin (CL) (Sigma-Aldrich, USA), were added exogenously to the assay system. Changes in the MIC of SS-CATH were then determined to evaluate its interactions with different lipid components.

Outer membrane permeability assay

The effect of SS-CATH on the outer membrane permeability of Gram-negative bacteria was evaluated using the fluorescent probe N-phenyl-1-naphthylamine (NPN) as previously described (Chen et al., 2023). Briefly, mid-logarithmic-phase ESBL-producing *E. coli* 4 cultures were diluted to 1×10^8 CFU/mL in MH broth and incubated with SS-CATH at the indicated concentrations. NPN (Sigma-Aldrich, USA) was then added to a final concentration of 10 μmol/L, and the mixtures were transferred to black 96-well plates and incubated at 37°C for 60 min in the dark. Fluorescence was measured immediately using a microplate reader (Tecan Group Ltd., Switzerland)with an excitation wavelength of 350 nm and an emission wavelength of 420 nm. PBS and Polymyxin B were used as the negative and positive controls, respectively. The experiments were performed in three independent biological replicates.

Inner membrane permeability assay

The effect of SS-CATH on bacterial inner membrane permeability was assessed using PI staining as previously described (Chen et al., 2023). Mid-logarithmic-phase ESBL-producing *E. coli* 4 cultures were diluted to 1×10^8 CFU/mL in MH broth and treated with SS-CATH at the indicated concentrations. PI was added to a final concentration of 5 μmol/L, and the mixtures were transferred to black 96-well plates and incubated at 37°C for 60 min in the dark. Fluorescence was then measured using a microplate reader (Tecan Group Ltd., Switzerland) with an excitation wavelength of 535 nm and an emission wavelength of 615 nm. PBS and

uncorrected proof

Triton X-100 served as the negative and positive controls, respectively. The experiments were performed in three independent biological replicates.

Cytoplasmic membrane depolarization assay

Cytoplasmic membrane depolarization was evaluated using the membrane potential-sensitive fluorescent probe 3,3′-dipropylthiadicarbocyanine iodide [$DiSC_3(5)$] (Sigma-Aldrich, USA) as previously described (Mwangi et al., 2025). Briefly, mid-logarithmic-phase ESBL-producing *E. coli* 4 cultures were diluted to 3×10^7 CFU/mL in the PBS and incubated with $DiSC_3(5)$ at a final concentration of 10 μmol/L for 30 min at 37°C in the dark to allow probe uptake and stabilization of the fluorescence signal. SS-CATH was then added at the indicated concentrations, and fluorescence was monitored continuously for 60 min using a microplate reader (Tecan Group Ltd., Switzerland) with an excitation wavelength of 622 nm and an emission wavelength of 670 nm. Fluorescence values were expressed as relative fluorescence units (RFU). Bacteria treated with PBS and Triton X-100 served as the negative and positive controls, respectively. The experiments were performed in three independent biological replicates.

Intracellular contents leakage assay

The leakage of intracellular macromolecules induced by SS-CATH was evaluated using an ultramicro ultraviolet–visible spectrophotometric method with minor modifications as previously described (Zhong et al., 2025). Briefly, mid-logarithmic-phase ESBL-producing *E. coli* 4 cultures were diluted to 1×10^9 CFU/mL in the appropriate culture medium and incubated with SS-CATH at the indicated concentrations at 37°C. At the designated time points, equal volumes of the bacterial suspensions were collected and centrifuged at 12 000 r/min (centrifuge radius: 8 cm) for 10 min at 4°C to remove cell debris. The supernatants were collected, and

uncorrected proof

their absorbance at 260 and 280 nm was measured using a NanoDrop™ One spectrophotometer (Thermo Scientific, USA) as an indicator of the relative amounts of released nucleic acids and proteins, respectively. The experiments were performed in three independent biological replicates.

Scanning electron microscopy (SEM)

The morphological changes of bacterial cells following SS-CATH treatment were examined by SEM with minor modifications as previously described (Zhang et al., 2025). Mid-logarithmic-phase ESBL-producing *E. coli* 4 cultures were diluted to 5×10^8 CFU/mL in the appropriate culture medium and incubated with SS-CATH at the indicated concentrations for 2 h at 37°C. The bacterial cells were then collected by centrifugation at 4°C, washed twice with PBS, and fixed overnight at 4°C in 2.5% glutaraldehyde. After fixation, the cells were washed three times with PBS and dehydrated through a graded ethanol series (50%, 70%, 80%, 90%, and 100%), with each step lasting 10 min. The samples were subsequently treated with a 1:1 (v/v) mixture of absolute ethanol and tert-butanol for 10 min, followed by 100% tert-butanol for 10 min. The dehydrated bacterial suspension was dropped onto clean glass slides and air-dried at room temperature. The samples were then sputter-coated with gold and examined using a Hitachi S-4800 scanning electron microscope (Hitachi High-Tech Corporation, Japan) at appropriate magnifications.

DNA gel retardation assay

The binding affinity of SS-CATH to ESBL-producing *E. coli* 4 genomic DNA was evaluated by agarose gel electrophoresis as previously described (Ma et al., 2020). Genomic DNA was extracted from the target bacterial strain using the TIANamp Bacteria DNA Kit (Tiangen Biotech Co., Ltd., China), and its purity and concentration were determined using a

Uncorrected proof

NanoDrop™ One spectrophotometer (Thermo Scientific, USA). The genomic DNA was then incubated with SS-CATH at the indicated concentrations for 30 min at 37°C to allow peptide–DNA binding. After incubation, 6×DNA loading buffer was added to each sample, and equal volumes were loaded onto a 1% agarose gel for electrophoretic separation. Genomic DNA without peptide treatment served as the negative control. The experiments were performed in three independent biological replicates. A representative gel image is shown, and similar results were obtained in three independent biological replicates.

To assess whether the DNA-binding activity of SS-CATH extends beyond bacterial genomic DNA, additional gel retardation assays were performed using CpG oligodeoxynucleotide 2395 (CpG ODN 2395) and genomic DNA isolated from RAW264.7 and HaCat cells. Each nucleic acid substrate was maintained at a final concentration of 50 μg/mL and incubated with SS-CATH at final concentrations of 50, 100, 150, 200, and 250 μg/mL, corresponding to nucleic acid-to-peptide mass ratios of 1:1, 1:2, 1:3, 1:4, and 1:5, respectively. Incubation and electrophoresis were performed as described above. Each nucleic acid substrate without SS-CATH served as the corresponding control.

Zeta potential assay

The interaction between SS-CATH and ESBL-producing *E. coli* 4 genomic DNA was further evaluated by zeta potential analysis. Genomic DNA was extracted from the target bacterial strain using the TIANamp Bacteria DNA Kit (Tiangen Biotech Co., Ltd., China), and its purity and concentration were determined using a NanoDrop™ One spectrophotometer (Thermo Scientific, USA). The genomic DNA was incubated with SS-CATH at the indicated concentrations for 30 min at 37°C under the same conditions as those used in the DNA gel retardation assay. The zeta potential of each sample was then measured using a Litesizer 500 Particle Analyzer (Anton Paar, Austria). Genomic DNA without peptide treatment served as

uncorrected proof

the negative control. All experiments were performed in three independent biological replicates.

Ethidium bromide (EB) displacement assay

The binding of SS-CATH to ESBL-producing *E. coli* 4 genomic DNA was further evaluated using an EB displacement assay. Bacterial genomic DNA was extracted from the target bacterial strain using the TIANamp Bacteria DNA Kit (Tiangen Biotech Co., Ltd., China), and its purity and concentration were determined using a NanoDrop™ One spectrophotometer (Thermo Scientific, USA). Genomic DNA was first incubated with EB at room temperature for 10 min to allow the formation of the EB–DNA complex. SS-CATH was then added at the indicated concentrations and incubated for an additional 30 min at 37°C. Fluorescence emission spectra were recorded from 560–660 nm using a multimode microplate reader (Tecan Group Ltd., Switzerland) with an excitation wavelength of 535 nm. Genomic DNA incubated with EB in the absence of peptide served as the negative control. All experiments were performed in three independent biological replicates.

LPS-binding assay

The binding affinity of SS-CATH to LPS was evaluated using a BODIPY-TR cadaverine (BC) displacement assay (MedChemExpress, USA). Briefly, LPS from *E. coli* O111:B4 (Sigma-Aldrich, USA) was diluted in PBS to a final concentration of 5 μg/mL. BC probe was then added to the LPS solution to a final concentration of 5 μmol/L, and the mixture was incubated at room temperature in the dark for 30 min to allow BC binding to LPS. After incubation, the LPS-BC complex was mixed with equal volumes of SS-CATH at various concentrations and further incubated at room temperature in the dark for 30 min. Fluorescence intensity was measured using a microplate reader (Tecan Group Ltd., Switzerland) at excitation/emission wavelengths of 580/620 nm. An increase in fluorescence intensity

Uncorrected proof

indicates displacement of BC from LPS by SS-CATH, reflecting the peptide's LPS-binding capacity. All experiments were performed in three independent biological replicates.

Detection of reactive oxygen species (ROS)

Intracellular ROS production was determined using the fluorescent probe 2′,7′-dichlorodihydrofluorescein diacetate (DCFH-DA) (Beyotime Biotechnology, China) as previously described (Zhao et al., 2025). Briefly, mid-logarithmic-phase ESBL-producing *E. coli* 4 cultures were diluted to 1×10^8 CFU/mL in the appropriate culture medium and incubated with 10 μmol/L DCFH-DA at 37°C for 30 min in the dark. After incubation, the bacterial cells were collected by centrifugation, washed two to three times with PBS to remove excess probe, and resuspended in PBS. SS-CATH was then added at the indicated concentrations, and the suspensions were incubated for an additional 1 h at 37°C in the dark. Following treatment, 200 μL of each bacterial suspension was transferred to a black 96-well plate, and fluorescence was measured using a microplate reader (Tecan Group Ltd., Switzerland) with an excitation wavelength of 488 nm and an emission wavelength of 525 nm. Bacteria treated with PBS and Polymyxin B served as the negative and positive controls, respectively. The experiments were performed in three independent biological replicates.

For the time-course analysis, DCFH-DA fluorescence was measured immediately after SS-CATH addition (defined as 0 min) and at 15, 30, 45, 60, 90, and 120 min. SS-CATH was tested at 0.5×, 1×, 2×, and 5×MIC, with PBS serving as the control. Three independent biological replicates were performed.

Measurement of hydroxyl radicals (•OH)

Intracellular •OH production was determined using the fluorescent probe hydroxyphenyl fluorescein (HPF) (Macklin, China) as previously described (Brochmann et al., 2014). Briefly,

Uncorrected proof

mid-logarithmic-phase ESBL-producing *E. coli* 4 cultures were diluted to 1×10^8 CFU/mL in the appropriate culture medium and incubated with 10 μmol/L HPF at 37°C for 30 min in the dark. After incubation, the bacterial cells were collected by centrifugation, washed two to three times with PBS to remove excess probe, and resuspended in PBS. SS-CATH was then added at the indicated concentrations, and the suspensions were incubated for an additional 1 h at 37°C in the dark. Following treatment, the bacterial suspensions were transferred to black 96-well plates, and fluorescence was measured using a microplate reader (Tecan Group Ltd., Switzerland) with an excitation wavelength of 490 nm and an emission wavelength of 515 nm. Bacteria treated with PBS and Polymyxin B served as the negative and positive controls, respectively. All experiments were performed in three independent biological replicates.

ROS scavenger assay

The roles of N-acetylcysteine (NAC) (Aladdin, China) and thiourea (TU) (Aladdin, China) in the antibacterial activity of SS-CATH were evaluated using ROS scavenging assays. Mid-logarithmic-phase ESBL-producing *E. coli* 4 cultures were diluted to 1×10^8 CFU/mL and divided into six groups: an untreated control, NAC alone, TU alone, SS-CATH alone, SS-CATH combined with NAC, and SS-CATH combined with TU. The samples were incubated at 37°C for 1 h. Bacterial survival was assessed qualitatively using a spot-plating assay, and intracellular ROS levels were measured using the DCFH-DA fluorescent probe. The experiments were performed in three independent biological replicates.

To assess whether NAC or TU affected bacterial membrane permeability or SS-CATH-induced membrane permeabilization, NPN and PI fluorescence were measured in bacteria treated with each scavenger in the absence or presence of SS-CATH. These measurements were performed in three independent biological replicates. Corresponding controls received an equal volume of PBS in place of the scavengers.

Uncorrected proof

In vivo therapeutic efficacy evaluation

All animal experiments were conducted in accordance with the relevant guidelines for the care and use of laboratory animals and were approved by the Institutional Animal Care and Use Committee of the Yantai Institute of Coastal Zone Research, Chinese Academy of Sciences(approval No. KJ-LL-029). Specific pathogen-free (SPF) BALB/c mice (6–8 weeks old, 20±2 g, equal numbers of males and females) were used in this study. All animals were acclimated for at least 72 h before the experiments. The group size was determined with reference to previous studies, with six mice per group (Xie et al., 2021).

To establish the murine peritonitis model, mice were intraperitoneally injected with 50 μL of ESBL-producing *E. coli* 4 suspension (1×10^8 CFU/mL). Two hours after infection, mice were weighed and allocated to four groups with comparable mean body weights (n=6 per group). Cages were labeled A–D, and the four treatments, PBS, Polymyxin B (10 mg/kg), SS-CATH (5 mg/kg), and SS-CATH (10 mg/kg), were randomly assigned to the coded groups. All treatments were administered by intraperitoneal injection at equal volumes. Survival was monitored daily for 7 days by personnel blinded to the treatment assignments, and the 7-day survival rate was used to evaluate the therapeutic efficacy.

For bacterial burden and histopathological analyses, mice were infected intraperitoneally with 50 μL of ESBL-producing *E. coli* 4 suspension (5×10^7 CFU/mL). Two hours after infection, mice were grouped and treatments were assigned using the same body-weight balancing and coded-group randomization procedure described above (n=6 per group). The assigned treatments were then administered. Twelve hours after drug administration, the mice were euthanized. Peritoneal lavage fluid and the heart, liver, spleen, lungs, and kidneys were aseptically collected. Tissue homogenates were serially diluted, plated on LB agar, and CFUs were quantified using an automatic colony counter (DTS3, Ze Xi Biotechnology, China). Liver and kidney tissues were additionally collected for hematoxylin and eosin (H&E) staining to

uncorrected proof

evaluate histopathological changes.

STATISTICAL ANALYSIS

All experiments were performed with at least three independent biological replicates. Continuous data are presented as mean±standard deviation (SD). Statistical significance was determined by one-way analysis of variance (ANOVA) followed by Tukey's post hoc test for multiple comparisons, or by two-tailed unpaired Student's *t*-test for comparisons between two groups. Survival curves were estimated using the Kaplan–Meier method and compared using the log-rank (Mantel–Cox) test. Bonferroni correction was applied to the three pairwise comparisons between the treatment groups and the PBS group. Animals surviving to the end of the 7-day observation period were right-censored. Analyses were conducted using GraphPad Prism v.9.0.

RESULTS

Identification and structural characterization of SS-CATH

Sea snakes have adapted to marine environments through a unique evolutionary history, making them a valuable source for the discovery of novel innate immune molecules. Cathelicidin precursor proteins typically consist of a conserved N-terminal signal peptide, a CLD, and a highly variable C-terminal mature peptide region (Bals & Wilson, 2003; Salnikov et al., 2025). To systematically identify sea snake cathelicidins, we collected annotated genome sequences from multiple sea snake species available in the NCBI database, including *A. laevis, H. cyanocinctus, H. major, H. elegans, and H. ornatus.* The conserved CLD was used as the query sequence for homology searches, leading to the identification of multiple cathelicidin precursor proteins. Structural analysis showed that all identified precursors possessed the

Uncorrected proof

characteristic signal peptide–cathelin domain–mature peptide architecture (Figure 1A). Besides, the mature peptides from *H. cyanocinctus*, *H. major, H. elegans and H. ornatus* were highly conserved (Figure 1A). Their signal peptides and cathelin domains also exhibited high sequence similarity, with only a few amino acid substitutions. These findings indicate limited sequence divergence among the four *Hydrophis* cathelicidin homologs, which may reflect recent common ancestry or possible functional constraint. Based on their origin and the remarkable conservation of the mature peptide sequences, we designated this mature peptide of sea snake cathelicidins as SS-CATH. Sequence BLAST analysis of the NCBI protein database revealed that SS-CATH exhibits 71% identity with cathelicidin-related peptide Oh-Cath-like from the terrestrial snake *Pantherophis guttatus* (XP_060540646.1), which in fact is a putative peptide by genomic annotation and its function remains unknown.

Helical wheel projection of full-length mature SS-CATH revealed a typical amphipathic architecture, with positively charged residues, including lysine (K) and arginine (R), clustered on one side of the helix, whereas hydrophobic residues, including valine (V), phenylalanine (F) and leucine (L), were distributed on the opposite side (Figure 1B). This distinct segregation of cationic and hydrophobic residues is a characteristic feature of many membrane-active AMPs and may facilitate electrostatic interactions with negatively charged bacterial membranes. The three-dimensional structure predicted by AlphaFold3 suggested that SS-CATH has a predominantly α-helical conformation, which is consistent with the amphipathic organization revealed by the helical wheel projection (Figure 1C). However, the experimentally determined secondary structure of SS-CATH was strongly dependent on the surrounding environment. CD spectroscopy showed that SS-CATH predominantly adopted a random-coil conformation in aqueous solution, whereas the addition of 60 mmol/L SDS, which mimics a membrane-associated environment, induced a marked transition toward an α-helical conformation, as indicated by the characteristic negative ellipticity at 208 and 222 nm (Figure

Uncorrected proof

1D). These findings indicate that although AlphaFold3 predicts an α-helical structure for SS-CATH, the peptide is not constitutively α-helical in solution and can undergo an environment-dependent conformational transition to an α-helical structure upon interaction with membrane-mimicking conditions. The physicochemical properties of SS-CATH are summarized in Figure 1E. SS-CATH is a 34-amino-acid peptide with a predicted molecular weight of 4144.15 Da, a theoretical pI of 10.93, a net charge of +11, and a GRAVY of −0.54. Collectively, these structural and physicochemical features indicate that SS-CATH is a highly cationic peptide with amphipathic characteristics and an environment-dependent secondary structure.

In vitro antibacterial activity of SS-CATH

To determine whether these structural features confer antimicrobial function, we first evaluated the antibacterial spectrum of SS-CATH. The MICs against both standard strains and clinical drug-resistant isolates were determined using the broth microdilution method. As shown in Table 1 and Figure 2A, SS-CATH exhibited potent antibacterial activity against a broad range of clinically relevant MDR bacteria, including *E. coli*, *A. baumannii*, *K. pneumoniae*, and *S. epidermidis*. As shown in the table, SS-CATH exhibited markedly stronger activity against Gram-negative bacteria (GM: 7.94 μg/mL) than against Gram-positive ones (GM: 46.22 μg/mL). This preference may be associated with the occurrence of these taxa in their gut and skin microbiota (Zhong et al., 2022, 2023), which could have favored the evolution of peptides with enhanced activity against these pathogens. Because ESBL-producing *E. coli* possesses a representative Gram-negative outer membrane and exhibits both multidrug resistance and robust persister formation, it was selected as the model strain for subsequent mechanistic studies (Macesic et al., 2025).

Consistent with the MIC results, growth curve analysis demonstrated that SS-CATH inhibited the growth of ESBL-producing *E. coli* 4 in a concentration-dependent manner (Figure

Uncorrected proof

2B). Notably, treatment at 1×MIC was sufficient to markedly suppress bacterial growth throughout the 18-h observation period, whereas 0.5×MIC only delayed bacterial regrowth. We next evaluated its bactericidal activity using a killing kinetic assay. As shown in Figure 2C, D, SS-CATH rapidly killed ESBL-producing *E. coli* 4 in a concentration-dependent manner. At 5×MIC, complete bacterial killing was achieved within 30 min. Even at 1×MIC, SS-CATH markedly reduced the number of viable bacteria after 180 min of treatment. Under the same conditions, Polymyxin B exhibited slower bactericidal kinetics than SS-CATH at 5×MIC. We further evaluated the short-term bactericidal activity of SS-CATH using SYTO-9/PI dual-fluorescence staining. As shown in Figure 2E, F, treatment with SS-CATH for 1 h resulted in the death of approximately 35% of ESBL-producing *E. coli* 4, which was comparable to the effect of Polymyxin B. We next assessed the propensity of SS-CATH to induce bacterial resistance through a serial passage experiment over 40 consecutive passages (Figure 2G). Ciprofloxacin rapidly induced bacterial resistance, with the MIC increasing approximately 6-fold by the 35th passage. In contrast, no appreciable increase in the MIC of SS-CATH was observed throughout the experiment, showing a resistance profile similar to that of Polymyxin B. These results suggest a low propensity for resistance development to SS-CATH in ESBL-producing *E. coli 4* under the tested conditions. Further evaluation across diverse strain backgrounds would help establish the broader applicability of this finding.

Stability and *in vitro* biocompatibility of SS-CATH

To evaluate whether SS-CATH retains antibacterial activity under physiological conditions relevant to *in vivo* application, we assessed the effects of physiological cations and protease treatment on its antimicrobial activity. The peptide was incubated with Na^+, K^+, Ca^{2+}, Fe^{3+}, Zn^{2+}, and NH_4^+, and changes in the MIC were determined. As shown in Figure 3A, $CaCl_2$ caused a slight reduction in the antibacterial activity of SS-CATH, whereas the other cations

uncorrected proof

produced no detectable change in MIC compared with the untreated control. These results indicate that SS-CATH retains stable antibacterial activity under physiologically relevant ionic conditions. To further assess salt tolerance, we evaluated the antibacterial activity of SS-CATH at NaCl concentrations ranging from 100 to 500 mmol/L. The MIC remained unchanged across all tested concentrations (Supplementary Figure S1), demonstrating that SS-CATH retains antibacterial activity under elevated NaCl conditions. We next evaluated the proteolytic stability of SS-CATH by incubating the peptide with trypsin, chymotrypsin, or pepsin and measuring changes in MIC (Figure 3B). The MIC increased in a concentration-dependent manner following treatment with each protease, indicating that proteolytic degradation gradually reduced antibacterial activity. Nevertheless, SS-CATH maintained measurable antibacterial activity after protease treatment. Collectively, these findings demonstrate that SS-CATH exhibits favorable functional stability under physiologically relevant conditions.

To evaluate its biocompatibility, we first assessed the hemolytic activity of SS-CATH against mammalian erythrocytes. Mouse erythrocytes were incubated with increasing concentrations of SS-CATH (12.5–200 μg/mL), and hemolysis was quantified. As shown in Figure 3C, hemolytic activity increased with peptide concentration but remained below 15% even at 200 μg/mL. At concentrations within the effective antibacterial range, SS-CATH exhibited minimal hemolytic activity. Cytotoxicity was further evaluated in HaCat and RAW264.7 cells using the MTT assay. As shown in Figure 3D, cell viability remained above 70% in both cell lines even at the highest tested concentration (200 μg/mL). Overall, SS-CATH exhibited low cytotoxicity toward mammalian cells even at 200 μg/mL, a concentration far exceeding its therapeutic MICs, supporting acceptable *in vitro* biocompatibility under the tested conditions.

Antibiofilm and anti-persister activities of SS-CATH

Uncorrected proof

As biofilm formation and persister survival are major contributors to chronic infections and antibiotic treatment failure (Pletzer et al., 2016), we assessed the ability of SS-CATH to eradicate established biofilms, inhibit biofilm formation, and eliminate persisters (Pan et al., 2025b). The ability of SS-CATH to eradicate mature biofilms was first evaluated using crystal violet staining and the TTC reduction assay (Figure 4A). Crystal violet staining was used to quantify the remaining biofilm biomass, whereas TTC reduction reflected the metabolic activity of viable bacteria within the biofilm. SS-CATH eradicated established biofilms in a concentration-dependent manner. Both residual biofilm biomass and TTC absorbance generally decreased with increasing SS-CATH concentration. Compared with PBS, the reduction in TTC absorbance was significant at 2×and 5×MIC. We next examined the inhibitory effect of SS-CATH on biofilm formation. As shown in Figure 4B, biofilm biomass was progressively reduced with increasing peptide concentration and reached the lowest level following treatment with 5×MIC SS-CATH. These results demonstrate that SS-CATH not only disrupts established biofilms but also effectively inhibits biofilm development during the early stages of bacterial adhesion and colonization.

Bacterial persisters can tolerate high concentrations of antibiotics (Etayash et al., 2020). To evaluate the activity of SS-CATH against rifampicin-induced persister cells, surviving cells were quantified by CFU counting after treatment with different concentrations of peptides (Figure 4C, D). High numbers of persisters were consistently detected in the PBS-treated control group. In contrast, the number of surviving persisters decreased progressively with increasing concentrations of SS-CATH, indicating a clear concentration-dependent effect. At 5×MIC, SS-CATH reduced the number of viable persisters to the lowest level, and its bactericidal activity was comparable to that of Polymyxin B. Collectively, these findings demonstrate that SS-CATH effectively eradicates established biofilms, inhibits biofilm formation, and exhibits potent bactericidal activity in the rifampicin-induced persister model,

Uncorrected proof

although the persister phenotype of the surviving population was not directly verified in this study.

Effects of SS-CATH on bacterial membrane integrity

Numerous studies have demonstrated that cationic AMPs accumulate on the bacterial surface and preferentially bind negatively charged membrane phospholipids through electrostatic interactions (Ganesan et al., 2023; Gong et al., 2023; Yang et al., 2022). To investigate the interactions of SS-CATH with representative bacterial membrane components, we examined the effects of exogenously added lipids on its antibacterial activity using a lipid competition assay. As shown in Figure 5A, the effects of different membrane lipids on the antibacterial activity of SS-CATH varied. The presence of LPS and CL resulted in a pronounced increase in the MIC of SS-CATH, whereas PC and PE had relatively limited effects. LPS and CL are negatively charged components associated with bacterial membranes, whereas PE is a zwitterionic phospholipid and PC is also zwitterionic. The interaction of SS-CATH with LPS was further supported by the BC displacement assay (Figure 5B). These findings suggest that negatively charged membrane components, particularly LPS and CL, may interact with SS-CATH and interfere with its antibacterial activity. However, because the lipid competition assay provides indirect evidence of lipid interaction rather than a direct measurement of binding affinity, these results should not be interpreted as direct evidence of preferential lipid-binding affinity. The observed lipid-dependent effects may contribute to the interaction of SS-CATH with bacterial membranes.

To investigate whether SS-CATH affects membrane fluidity, we measured the GP value following peptide treatment. As shown in Figure 5C, the GP value increased significantly in a concentration-dependent manner, indicating that SS-CATH reduced bacterial membrane fluidity.

Uncorrected proof

Changes in membrane permeability are a hallmark of membrane damage, and cationic AMPs often disrupt membrane integrity after accumulating on the bacterial surface (Chen et al., 2025). We first evaluated the effect of SS-CATH on outer membrane permeability using the NPN uptake assay. As shown in Figure 5D, NPN fluorescence increased in a concentration-dependent manner as the concentration of SS-CATH increased from 0.5×MIC to 5×MIC, indicating progressive disruption of outer membrane integrity. We next assessed inner membrane damage using PI staining. As shown in Figure 5E, SS-CATH increased PI fluorescence in a concentration-dependent manner. At 5×MIC, PI fluorescence exceeded that induced by Triton X-100. These results demonstrate that SS-CATH effectively disrupts the bacterial inner membrane. Disruption of the cytoplasmic membrane is commonly accompanied by dissipation of the membrane potential. We therefore monitored changes in membrane potential using the voltage-sensitive fluorescent probe $DiSC_3(5)$. As shown in Figure 5F, SS-CATH increased $DiSC_3(5)$ fluorescence at 1×, 2×, and 5×MIC, indicating dissipation of the bacterial membrane potential and disruption of transmembrane ion homeostasis.

To further evaluate membrane disruption by SS-CATH, we measured the release of intracellular macromolecules by monitoring the absorbance of culture supernatants at OD_{260} and OD_{280}, which reflect the leakage of nucleic acids and proteins, respectively. As shown in Figure 5G, H, only minimal increases in OD_{260} and OD_{280} were observed in the untreated control during the 4 h incubation period, indicating that the bacterial membrane remained intact with negligible intracellular leakage. In contrast, treatment with SS-CATH at 1×MIC, 2×MIC, and 5×MIC resulted in progressive increases in both OD_{260} and OD_{280} over time. The extent of macromolecular leakage also increased in a concentration-dependent manner, with the 5×MIC group showing substantially higher leakage than the 1×MIC and 2×MIC groups. Membrane damage was further visualized by SEM. Untreated bacteria exhibited intact rod-shaped morphology with smooth cell surfaces. In contrast, SS-CATH-treated cells displayed

Uncorrected Proof

pronounced membrane shrinkage, surface collapse, structural disruption, and leakage of intracellular contents (Figure 5I). These morphological alterations provide direct evidence that SS-CATH severely compromises bacterial membrane integrity.

Collectively, these findings suggest that interactions with bacterial membrane lipids contribute to the membrane-disrupting activity of SS-CATH. It subsequently disrupts both the outer and inner membranes, alters membrane organization, dissipates the membrane potential, and promotes the leakage of intracellular macromolecules. These membrane-disrupting effects are consistent with the rapid bactericidal activity of SS-CATH.

DNA binding and oxidative stress induction by SS-CATH

Some AMPs have been reported to translocate across bacterial membranes and subsequently bind to intracellular DNA, thereby contributing to their bactericidal activity (Li et al., 2026b). The interaction of SS-CATH with purified bacterial genomic DNA was first examined using an agarose gel retardation assay. Bacterial genomic DNA was incubated with increasing concentrations of SS-CATH (25–125 μg/mL) while the DNA concentration was kept constant at 25 μg/mL. As shown in Figure 6A, when the DNA-to-peptide ratio reached 1:2, part of the DNA was retained in the loading well. At a DNA-to-peptide ratio of 1:5, DNA was completely retained in the loading well. This result indicated a concentration-dependent interaction between SS-CATH and bacterial genomic DNA. We next examined changes in DNA surface charge after peptide binding using zeta potential analysis (Figure 6B). As the concentration of SS-CATH increased, the negative zeta potential was progressively neutralized and shifted toward more neutral values in a concentration-dependent manner, indicating electrostatic binding between the cationic peptide and bacterial DNA. Furthermore, an EB fluorescence displacement assay further confirmed the DNA-binding ability of SS-CATH (Figure 6C), which was consistent with the gel retardation and zeta potential results. To further

Uncorrected proof

assess the substrate specificity of SS-CATH binding, we examined its interactions with CpG ODN 2395 and genomic DNA isolated from RAW264.7 and HaCat cells. SS-CATH retarded the electrophoretic migration of all three substrates. Free-migrating nucleic acid bands were no longer detectable at nucleic acid-to-peptide mass ratios of 1:4, 1:2, and 1:2 for CpG ODN 2395, RAW264.7 genomic DNA, and HaCat genomic DNA, respectively (Supplementary Figure S2A–C). These findings indicate that SS-CATH binding is not restricted to bacterial genomic DNA and support a contribution of nonspecific electrostatic interactions to its DNA-binding activity.

Previous studies have reported that some AMPs can induce oxidative stress in bacteria (Zhang et al., 2026), and ROS contribute to their bactericidal activity (Song et al., 2026). To investigate whether SS-CATH could trigger a similar oxidative response, intracellular ROS levels were measured using the DCFH-DA probe. As shown in Figure 6D, SS-CATH increased intracellular ROS abundance in a concentration-dependent manner. Importantly, at 1×, 2×, and 5×MIC, SS-CATH produced higher DCFH-DA fluorescence than Polymyxin B at the corresponding MIC multiples, suggesting a more pronounced oxidative stress response in SS-CATH-treated bacteria. Time-course analysis further showed that DCFH-DA fluorescence generally increased over the 120-min observation period in SS-CATH-treated bacteria, whereas the PBS control showed only minor changes (Supplementary Figure S3). Considered alongside the time-kill and membrane-leakage profiles (Figures 2C, D and 5G, H), these findings suggest that ROS accumulation accompanies the membrane-disrupting and bactericidal effects of SS-CATH. Cellular ROS encompass multiple components including superoxide anion, hydrogen peroxide, and hydroxyl radical (•OH) (Imlay, 2013). Among them, •OH is a highly reactive species that can inflict severe damage to biomacromolecules and is closely associated with bacterial cell death (Yi et al., 2025). We further measured intracellular •OH production using the HPF fluorescent probe. SS-CATH induced evident •OH generation

Uncorrected proof

at all tested concentrations, further confirming that SS-CATH could initiate oxidative stress within bacterial cells. To further verify the contribution of oxidative stress in the antibacterial action of SS-CATH, rescue experiments were performed using N-acetylcysteine (NAC), a ROS scavenger, and thiourea (TU), a hydroxyl radical scavenger (Figure 6F, G). Treatment with SS-CATH alone markedly increased intracellular ROS levels and significantly reduced bacterial survival. In contrast, the addition of NAC or TU markedly reduced ROS fluorescence and restored bacterial viability, as reflected by a substantial increase in colony density. NAC or TU alone did not visibly reduce colony formation compared with the PBS control. We further examined whether NAC or TU could interfere with SS-CATH activity by altering bacterial membrane permeability. Neither scavenger significantly altered NPN or PI fluorescence when used alone compared with PBS (Supplementary Figure S4A, B), or when combined with SS-CATH compared with SS-CATH alone (Supplementary Figure S4C, D). These findings suggest that the observed rescue was not accompanied by a detectable reduction in SS-CATH-induced membrane permeabilization and, together with the reduction in ROS fluorescence, support a contribution of oxidative stress to SS-CATH-mediated bacterial killing. Collectively, these findings suggest the DNA-binding capacity of SS-CATH and its ability to induce bacterial oxidative stress.

In vivo therapeutic activity of SS-CATH

To further evaluate the therapeutic potential of SS-CATH *in vivo*, a murine systemic peritonitis model induced by ESBL-producing *E. coli* 4 was established (Figure 7A). Mice were initially intraperitoneally challenged with 50 μL of bacterial suspension containing 1×10^8 CFU/mL ESBL-producing *E. coli* 4. Two hours after infection, mice were allocated to groups with comparable mean body weights, and treatments were randomly assigned to the coded groups as described in the Methods. The assigned treatments were administered at equal

Uncorrected proof

intraperitoneal injection volumes. Survival was monitored for 7 days. As shown in Figure 7B, mice in the PBS-treated group rapidly succumbed to infection and all died within day 1. In contrast, all mice treated with SS-CATH at either 5 mg/kg or 10 mg/kg survived throughout the observation period, corresponding to a 100% survival rate.

In a parallel experiment, mice were euthanized 12 h after drug administration, and bacterial burdens in the heart, liver, spleen, lung, kidney, and peritoneal lavage fluid were quantified by CFU counting. As shown in Figure 7C–H, high bacterial burdens were detected in all examined tissues and the peritoneal lavage fluid of the PBS-treated group. SS-CATH reduced bacterial burdens in the examined organs and peritoneal lavage fluid, with a dose-dependent trend in most samples. In some organs, the reductions in bacterial burdens even approached those observed with Polymyxin B, indicating that SS-CATH effectively eliminated MDR bacteria from multiple organs and limited bacterial dissemination *in vivo*.

Histopathological analysis further supported the therapeutic efficacy of SS-CATH. H&E staining revealed extensive inflammatory cell infiltration, vacuolar degeneration, and tissue damage in the liver and kidney of PBS-treated mice (Figure 7I). These pathological changes were progressively alleviated following SS-CATH treatment in a dose-dependent manner. Collectively, these results demonstrate that SS-CATH exhibits potent therapeutic activity against MDR Gram-negative bacterial infection *in vivo*. It effectively reduces bacterial burdens, alleviates tissue injury, and improves the survival of infected mice, highlighting its potential as a candidate for the treatment of MDR bacterial infections.

DISCUSSION

Sea snakes represent one lineage of reptiles that have fully adapted to marine environments. Their secondary transition from terrestrial to marine environments was accompanied by profound changes in salinity, osmotic pressure, and pathogen composition

Uncorrected proof

(Ludington et al., 2023; Ludington & Sanders, 2021). In marine environments, the high microbial load of seawater and the increased risk of wound infection impose persistent selective pressures on the innate immune system (Baker-Austin et al., 2018). The presence of Gram-negative taxa in the gut and skin microbiota of sea snakes, together with the association of several of these taxa with skin ulceration (Zhong et al., 2022, 2023), may have driven the evolution of cationic AMPs with enhanced activity against Gram-negative bacteria (Ludington et al., 2023). Compared with conventional bioactivity-guided peptide discovery, genome-guided mining provides an efficient strategy for identifying structurally novel AMPs from an evolutionary perspective (Kumar et al., 2024; Szymczak et al., 2025). To date, only a handful of sea snake-derived AMPs have been experimentally characterized. These peptides predominantly belong to the cathelicidin family and display potent activity against bacterial pathogens. These findings support the hypothesis that immune peptides of aquatic vertebrates may undergo adaptive evolution under long-term environmental selection pressure (Gao et al., 2025).

In this study, we systematically characterized the structural features, antibacterial activity, mechanism of action, and *in vivo* efficacy of SS-CATH. Structural analysis showed that SS-CATH is a cationic, amphipathic peptide capable of adopting an α-helical conformation under membrane-mimicking conditions. Antibacterial assays demonstrated that SS-CATH exhibited potent, rapid, and concentration-dependent bactericidal activity against MDR Gram-negative bacteria, including ESBL-producing *E. coli*, *K. pneumoniae*, and *A. baumannii*. Mechanistically, SS-CATH disrupted bacterial membrane integrity by targeting membrane lipids, exhibited DNA-binding activity *in vitro*, indicating a potential interaction between SS-CATH and bacterial genomic DNA, and induced oxidative stress, thereby exerting multitarget antibacterial activity. Previous work on LL-37 has implicated perturbation of the bacterial electron transport chain in peptide-induced oxidative stress (Choi et al., 2017). Given the

Uncorrected proof

membrane-disrupting activity of SS-CATH, interference with membrane-associated respiratory processes may likewise contribute to the observed ROS accumulation. Consistent with this mechanism, SS-CATH showed a low propensity to induce resistance after 40 serial passages. In a murine peritonitis model, SS-CATH significantly improved survival, reduced bacterial burdens, and alleviated tissue injury. Although SS-CATH showed acceptable *in vitro* biocompatibility, further *in vivo* safety evaluation is needed. Its binding to CpG ODN 2395 and mammalian genomic DNA indicates that its DNA-binding activity extends beyond bacterial DNA, consistent with a contribution of nonspecific electrostatic interactions. Potential interactions with host-cell DNA should therefore be considered in these further safety evaluations. Collectively, these findings demonstrate that SS-CATH exhibits potent antibacterial activity against MDR Gram-negative pathogens both *in vitro* and *in vivo*, highlighting its potential as a promising antimicrobial candidate.

Cathelicidin AMPs are key effector molecules of vertebrate innate immunity. Their mature peptide regions typically exhibit high sequence diversity among species, which is considered an evolutionary outcome of adaptation to specific pathogen pressures in different ecological niches (Whelehan et al., 2014). However, SS-CATH shows an identical mature peptide sequence in four species of the genus *Hydrophis* (*H. cyanocinctus, H. major, H. elegans and H. ornatus)*. This conservation should be considered in the context of their close phylogenetic relationship and the sequence diversity reported for the broader cathelicidin family (Wang et al., 2023). From an evolutionary perspective, conservation of the mature peptide sequence often implies functional constraint (Worth et al., 2009). Functionally, SS-CATH simultaneously fulfills multiple roles: maintaining antibacterial activity under the tested elevated NaCl conditions, covering diverse pathogens through synergistic multi-target mechanisms, and showing acceptable *in vitro* biocompatibility. The observed ionic tolerance may be relevant to the antimicrobial function of SS-CATH in saline marine environments,

Uncorrected proof

although the tested conditions do not reproduce the full ionic composition of seawater. The maintenance of these functional properties may impose constraints on sequence variation. Mutations that compromise these properties could be disfavored by purifying selection. SS-CATH may function as a broad-spectrum defense molecule, with its activity against Gram-negative bacteria potentially contributing to protection against opportunistic infections in sea snakes. For such generalist molecules, the maintenance of an effective sequence may favor functional conservation (De La Fuente-Núñez et al., 2017; Lazzaro et al., 2020). The close relationship among these *Hydrophis* species also raises the possibility that the observed conservation reflects recent common ancestry. Overall, the conservation of SS-CATH may reflect recent common ancestry and purifying selection, while adaptive retention and functional optimization remain possible explanations.

This study adopts the perspectives of zoology and evolutionary immunology. It characterizes the molecular features and bactericidal activities of SS-CATH, a conserved sea snake cathelicidin, and explores their potential evolutionary implications. Unlike previous studies that merely regarded sea snake AMPs as drug candidates, our work offers two key contributions. It provides rational strategies for developing new therapeutics against clinical Gram-negative drug-resistant infections. It also provides a basis for further investigation of the ecological and evolutionary roles of innate immune peptides in marine reptiles.

SUPPLEMENTARY DATA

Supplementary data to this article can be found online.

COMPETING INTERESTS

The authors declare that they have no competing interests.

AUTHORS' CONTRIBUTIONS

Y.P.W. and P.S. conceived and supervised the project. M.L.X. and S.Y.L. designed and

uncorrected proof

conducted the experiments, performed the data analysis, and wrote the manuscript. Z.K.X. assisted in SS-CATH sequence mining and bioinformatic analyses. Z.Z.L. assisted with the *in vivo* and *in vitro* antibacterial assays. Y.X.S., X.J.K. and J.J.Z. assisted with the manuscript writing. All authors read and approved the final version of the manuscript.

ACKNOWLEDGEMENTS

This work was supported by the National Natural Science Foundation of China (U24A20812 to Y.P.W., 32401067 to J.J.Z., and 32500419 to X.J.K.), Shandong Provincial Natural Science Foundation (ZR2025QC242 to X.J.K.), Natural Science Foundation of Yantai (ZR2025Q013 to J.J.Z.), and the Special Fund for the Scholar Program of Yantai to Y.P.W.

REFERENCES

Baker-Austin C, Oliver JD, Alam M, et al. 2018. *Vibrio* spp. infections. *Nature Reviews Disease Primers*, **4**(1): 8.

Bals R, Wilson JM. 2003. Cathelicidins–a family of multifunctional antimicrobial peptides. *Cellular and Molecular Life Sciences*, **60**(4): 711–720.

Bessa LJ, Ferreira M, Gameiro P. 2018. Evaluation of membrane fluidity of multidrug-resistant isolates of *Escherichia coli* and *Staphylococcus aureus* in presence and absence of antibiotics. *Journal of Photochemistry and Photobiology B: Biology*, **181**: 150–156.

Brochmann RP, Toft A, Ciofu O, et al. 2014. Bactericidal effect of colistin on planktonic *Pseudomonas aeruginosa* is independent of hydroxyl radical formation. *International Journal of Antimicrobial Agents*, **43**(2): 140–147.

Bucataru C, Ciobanasu C. 2024. Antimicrobial peptides: opportunities and challenges in overcoming resistance. *Microbiological Research*, **286**: 127822.

Chai J, Chen X, Ye T, et al. 2021. Characterization and functional analysis of cathelicidin-MH, a novel frog-derived peptide with anti-septicemic properties. *eLife*, **10**: e64411.

Uncorrected proof

Chen X, Song M, Tian L, et al. 2025. A plant peptide with dual activity against multidrug-resistant bacterial and fungal pathogens. *Science Advances*, **11**(12): eadt8239.

Chen Y, Yong M, Li M, et al. 2023. A hydrophilic polyimidazolium antibiotic targeting the membranes of Gram-negative bacteria. *Journal of Antimicrobial Chemotherapy*, **78**(10): 2581–2590.

Choi H, Yang Z, Weisshaar JC. 2017. Oxidative stress induced in *E. coli* by the human antimicrobial peptide LL-37. *PLOS Pathogens*, **13**(6): e1006481.

De La Fuente-Núñez C, Silva ON, Lu TK, et al. 2017. Antimicrobial peptides: role in human disease and potential as immunotherapies. *Pharmacology & Therapeutics*, **178**: 132–140.

Etayash H, Qian Y, Pletzer D, et al. 2020. Host defense peptide-mimicking amphiphilic β-peptide polymer (Bu:DM) exhibiting anti-biofilm, immunomodulatory, and in vivo anti-infective activity. *Journal of Medicinal Chemistry*, **63**(21): 12921–12928.

Ganesan N, Mishra B, Felix L, et al. 2023. Antimicrobial peptides and small molecules targeting the cell membrane of *Staphylococcus aureus*. *Microbiology and Molecular Biology Reviews*, **87**(2): e0003722.

Gao B, Yang N, Teng D, et al. 2025. Marine antimicrobial peptides: advances in discovery, multifunctional mechanisms, and therapeutic translation challenges. *Marine Drugs*, **23**(12): 463.

Giacometti A, Cirioni O, Barchiesi F, et al. 2000. In vitro susceptibility tests for cationic peptides: comparison of broth microdilution methods for bacteria that grow aerobically. *Antimicrobial Agents and Chemotherapy*, **44**(6): 1694–1696.

Gong H, Hu X, Zhang L, et al. 2023. How do antimicrobial peptides disrupt the lipopolysaccharide membrane leaflet of Gram-negative bacteria? *Journal of Colloid and Interface Science*, **637**: 182–192

Haney EF, Trimble MJ, Cheng JT, et al. 2018. Critical assessment of methods to quantify

Uncorrected proof

biofilm growth and evaluate antibiofilm activity of host defence peptides. *Biomolecules*, **8**(2): 29.

Hanstein S, Grochow T, Mötzing M, et al. 2025. Comparative evaluation of antimicrobial peptides: effect on formation, metabolic activity and viability of Klebsiella pneumoniae biofilms. *Frontiers in Microbiology*, **16**: 1548362.

Imlay JA. 2013. The molecular mechanisms and physiological consequences of oxidative stress: lessons from a model bacterium. *Nature Reviews Microbiology*, **11**(7): 443–454.

Kavela S, Kakkerla S, Thupurani MK. 2025. Broad-spectrum antimicrobial activity and in vivo efficacy of SK1260 against bacterial pathogens. *Frontiers in Microbiology*, **16**: 1553693.

Kumar N, Bhagwat P, Singh S, et al. 2024. A review on the diversity of antimicrobial peptides and genome mining strategies for their prediction. *Biochimie*, **227**(Pt A): 99–115.

Lazzaro BP, Zasloff M, Rolff J. 2020. Antimicrobial peptides: application informed by evolution. *Science*, **368**(6490): eaay9012.

Li A, Wang J, Sun K, et al. 2021. Two reference-quality sea snake genomes reveal their divergent evolution of adaptive traits and venom systems. *Molecular Biology and Evolution*, **38**(11): 4867–4883.

Li SY, Wang K, Shi W, et al. 2026a. Vm-MSI: a vancomycin-antimicrobial peptide conjugate combating resistant bacteria and broadening the antimicrobial spectrum. *Advanced Science*, **13**(11): e03023.

Li YT, Wei TC, Yuan JX, et al. 2026b. Biomimetic antimicrobial peptides against gram-positive bacteria. *Biomaterials*, **329**: 123916.

Ludington AJ, Hammond JM, Breen J, et al. 2023. New chromosome-scale genomes provide insights into marine adaptations of sea snakes (Hydrophis: Elapidae). *BMC Biology*, **21**(1): 284.

Ludington AJ, Sanders KL. 2021. Demographic analyses of marine and terrestrial snakes

Uncorrected proof

(Elapidae) using whole genome sequences. *Molecular Ecology*, **30**(2): 545–554.

Ma L, Xie X, Liu H, et al. 2020. Potent antibacterial activity of MSI-1 derived from the magainin 2 peptide against drug-resistant bacteria. *Theranostics*, **10**(3): 1373–1390.

Ma Y, Guo Z, Xia B, et al. 2022. Identification of antimicrobial peptides from the human gut microbiome using deep learning. *Nature Biotechnology*, **40**(6): 921–931.

Macesic N, Uhlemann AC, Peleg AY. 2025. Multidrug-resistant Gram-negative bacterial infections. *The Lancet*, **405**(10474): 257–272.

Magiorakos AP, Srinivasan A, Carey RB, et al. 2012. Multidrug-resistant, extensively drug-resistant and pandrug-resistant bacteria: an international expert proposal for interim standard definitions for acquired resistance. *Clinical Microbiology and Infection*, **18**(3): 268–281.

Mhlongo JT, Waddad AY, Albericio F, et al. 2023. Antimicrobial peptide synergies for fighting infectious diseases. *Advanced Science*, **10**(26): e2300472.

Mwangi J, Tadese DA, Wang Y, et al. 2025. Integrating a cationic backbone with a hydrophobic core: a structure-function strategy for designing self-assembling antimicrobial peptides with enhanced activity. *Zoological Research*, **46**(5): 1203–1218.

Pan HY, Ye RW, Han S, et al. 2025a. Discovery of a novel sea snake antimicrobial peptide Hydrostatin-AMP3 with dual-mechanism against multidrug-resistant *Klebsiella pneumoniae*. *European Journal of Medicinal Chemistry*, **293**: 117696.

Pan Y, Liu H, Liu Y, et al. 2025b. Antimicrobial peptide-antibiotic synergy exerts anti-streptococcus suis infection by membrane disruption, ROS induction and biofilm inhibition. *International Immunopharmacology*, **161**: 115053.

Peel E, Gonsalvez A, Hogg CJ, et al. 2025. Marsupial cathelicidins: characterization, antimicrobial activity and evolution in this unique mammalian lineage. *Frontiers in Immunology*, **16**: 1524092.

Uncorrected proof

Pletzer D, Coleman SR, Hancock RE. 2016. Anti-biofilm peptides as a new weapon in antimicrobial warfare. *Current Opinion in Microbiology*, **33**: 35–40.

Salnikov E, Adélaïde M, Ramos-Martín F, et al. 2025. Cathelicidin-BF: a potent antimicrobial peptide leveraging charge and phospholipid recruitment against multidrug-resistant clinical bacterial isolates. *Journal of the American Chemical Society*, **147**(13): 11199–11215.

Song Y, Ye Z, Wang Y. 2026. Metabolite-driven reprogramming of bacterial persisters: mechanisms and therapeutic opportunities for overcoming antibiotic tolerance. *Drug Resistance Updates*, **84**: 101322.

Szymczak P, Zarzecki W, Wang J, et al. 2025. AI-driven antimicrobial peptide discovery: mining and generation. *Accounts of Chemical Research*, **58**(12): 1831–1846.

Tajer L, Paillart JC, Dib H, et al. 2024. Molecular mechanisms of bacterial resistance to antimicrobial peptides in the modern era: an updated review. *Microorganisms*, **12**(7): 1259.

Wang S, Fan L, Pan H, et al. 2023. Identification and characterization of a novel cathelicidin from *Hydrophis cyanocinctus* with antimicrobial and anti-inflammatory activity. *Molecules*, **28**(5): 2082.

Wei L, Gao J, Zhang S, et al. 2015. Identification and characterization of the first cathelicidin from sea snakes with potent antimicrobial and anti-inflammatory activity and special mechanism. *Journal of Biological Chemistry*, **290**(27): 16633–16652.

Whelehan CJ, Barry-Reidy A, Meade KG, et al. 2014. Characterisation and expression profile of the bovine cathelicidin gene repertoire in mammary tissue. *BMC Genomics*, **15**: 128.

Worth CL, Gong S, Blundell TL. 2009. Structural and functional constraints in the evolution of protein families. *Nature Reviews Molecular Cell Biology*, **10**(10): 709–720.

Xie J, Zhou M, Qian Y, et al. 2021. Addressing MRSA infection and antibacterial resistance

Uncorrected proof

with peptoid polymers. *Nature Communications*, **12**(1): 5898.

Xuan J, Feng W, Wang J, et al. 2023. Antimicrobial peptides for combating drug-resistant bacterial infections. *Drug Resistance Updates*, **68**: 100954.

Yadav N, Chauhan VS. 2024. Advancements in peptide-based antimicrobials: a possible option for emerging drug-resistant infections. *Advances in Colloid and Interface Science*, **333**: 103282.

Yang H, Wang L, Yuan L, et al. 2022. Antimicrobial peptides with rigid linkers against Gram-negative bacteria by targeting lipopolysaccharide. *Journal of Agricultural and Food Chemistry*, **70**(50): 15903–15916.

Ye Z, Fu L, Li S, et al. 2024. Synergistic collaboration between AMPs and non-direct antimicrobial cationic peptides. *Nature Communications*, **15**(1): 7319.

Yi J, Liu J, Gao B, et al. 2025. Humidity-triggered sterilization mechanism of CuCeOx: hydroxyl radical-mediated protein synthesis inhibition and energy depletion. *Journal of Hazardous Materials*, **497**: 139581.

Zhang J, Chu A, Yang P, et al. 2025. High therapeutic index α-helical antimicrobial peptides with repetitive subunit structures against multidrug-resistant bacteria. *European Journal of Medicinal Chemistry*, **298**: 117996.

Zhang M, Ouyang J, Fu L, et al. 2022. Hydrophobicity determines the bacterial killing rate of α-helical antimicrobial peptides and influences the bacterial resistance development. *Journal of Medicinal Chemistry*, **65**: 14701–14720.

Zhang P, Ye Z, Dou H, et al. 2026. Identification and characterization of broad-spectrum cathelicidin family antimicrobial peptides from the pygmy sperm whale *Kogia breviceps*. *Biochemical Pharmacology*, **245**: 117675.

Zhao L, Wang Y, Jiang J, et al. 2025. Evaluation of LLM-generated peptide as foundation template for discovery of effective encrypted AMPs against clinical superbugs.

Uncorrected proof

Microbiology Spectrum, **13**(10): e0150425.

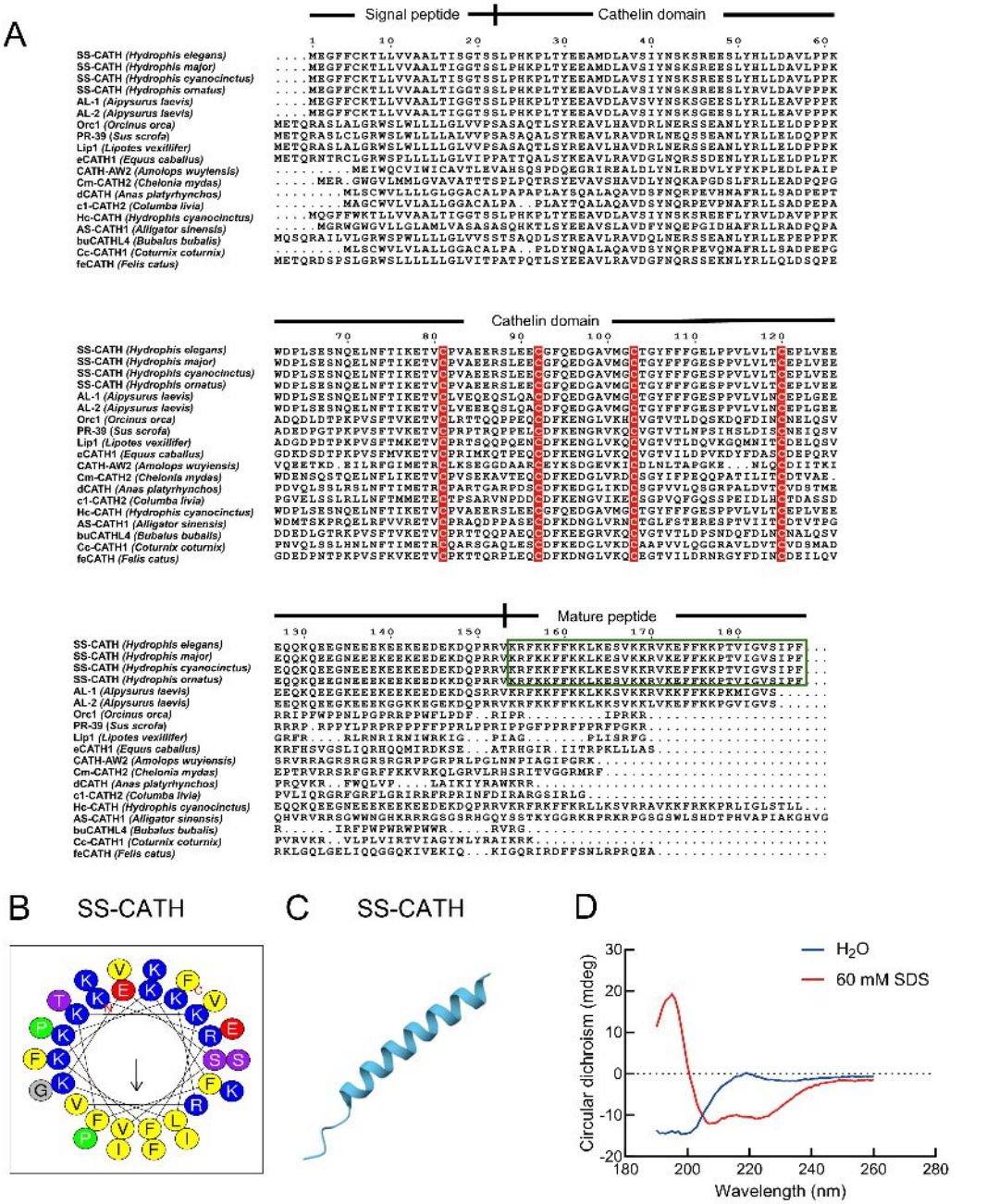
Zhong C, He Y, Zou J, et al. 2025. An antimicrobial peptide as a potential therapy for bacterial pneumonia that alleviates antimicrobial resistance. *Nature Communications*, **16**(1): 10488.

Zhong J, Guo K, Liao ZL, et al. 2022. Comparative analysis of the gut microbiota composition between two sea snakes, *Hydrophis curtus* and *Hydrophis cyanocinctus*. *Coral Reefs*, **41**: 53–62.

Zhong J, Guo K, Liao ZL, et al. 2023. Comparative analysis of the skin microbiota between two sea snakes, *Hydrophis cyanocinctus* and *Hydrophis curtus*, with versus without skin ulcer. *Coral Reefs*, **42**: 743–753.

uncorrected proof

FIGURE



Peptide	Sequence	H	Z	L	pI	MW
SS-CATH	KRFKKFFKKLKESVKKRVKEFFKKPTVIGVSIPF	-0.54	+11	34	10.93	4144.15

Figure 1. Sequence and structural characterization of SS-CATH. A: Multiple sequence alignment of cathelicidin precursors derived from representative vertebrate species covering

Zoological Research

sea snakes, other reptiles, mammals and amphibians. Sequences from several closely related sea snake species were included to analyze the conservation of mature SS-CATH. The region corresponding to mature peptide SS-CATH is highlighted within the green box. Four representative conserved cysteine residues within the cathelicidin domain are marked in red. The signal peptide and cathelin domain are annotated above the alignment. B: Helical wheel projection of full-length mature SS-CATH generated by HeliQuest, showing the distribution of positively charged and hydrophobic residues. C: Three-dimensional structure of SS-CATH predicted by AlphaFold3. D: Circular dichroism (CD) spectra of SS-CATH in H_2O and 60 mmol/L SDS. E: Amino acid sequence and physicochemical properties of SS-CATH, including peptide length (L), net charge (Z), GRAVY (H), isoelectric point (pI), and molecular weight (MW).

uncorrected proof

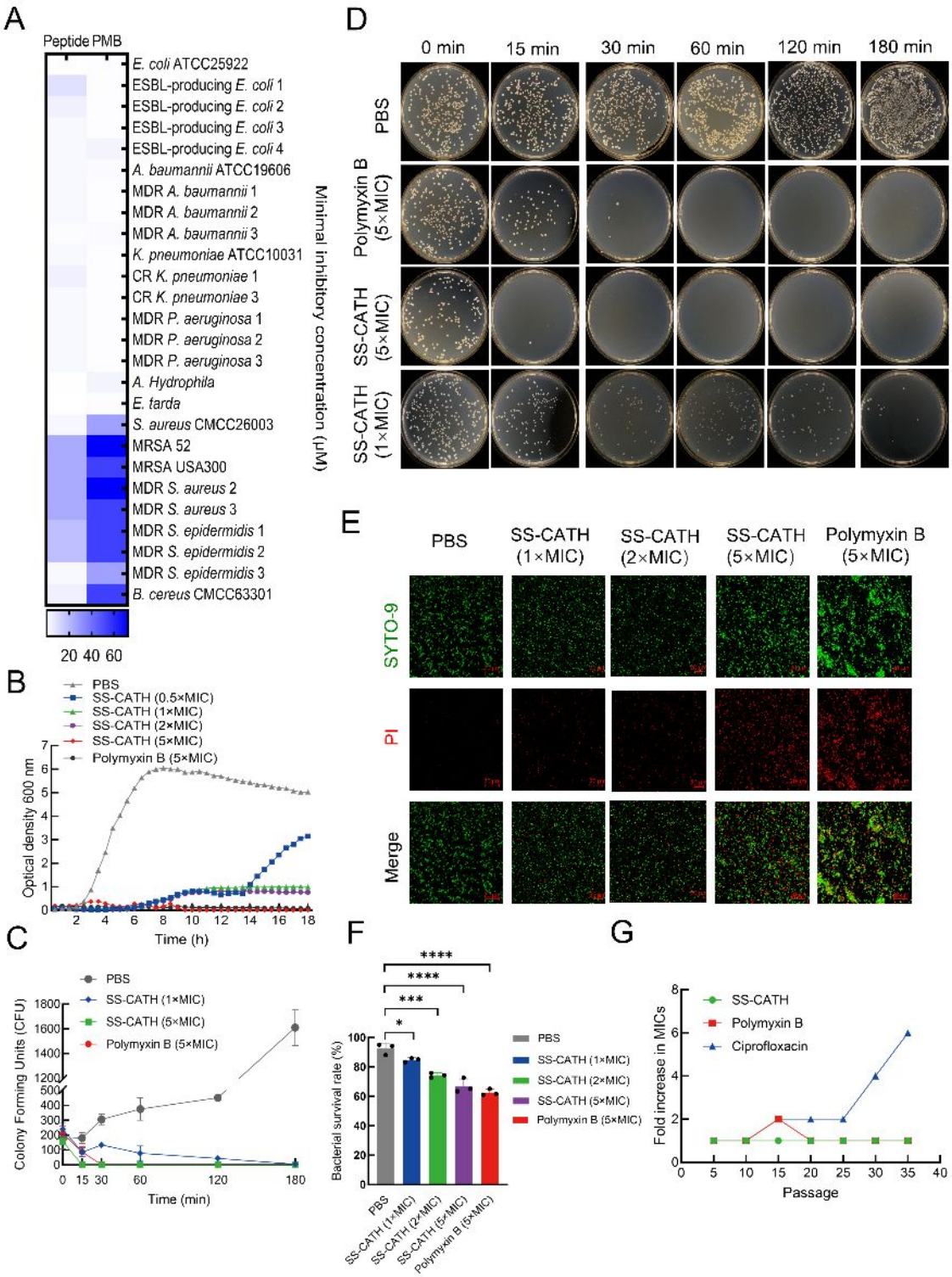


Figure 2. *In vitro* antibacterial activity and resistance-inducing potential of SS-CATH.

A: Heatmap showing the MICs of SS-CATH and Polymyxin B against reference strains and MDR clinical isolates. B: Growth curves of ESBL-producing *E. coli* 4 treated with SS-CATH at 0.5×, 1×, 2×, and 5×MIC. Polymyxin B at 5×MIC served as the positive control, and PBS

served as the negative control. C: Time-kill kinetics of SS-CATH (1× and 5×MIC) and Polymyxin B (5×MIC) against ESBL-producing *E. coli* 4, determined by CFU counting. D: Representative agar plates showing bacterial survival during the time-kill assay following treatment with SS-CATH or Polymyxin B. E: Representative SYTO-9/PI fluorescence images of ESBL-producing *E. coli* 4 following treatment with SS-CATH at the indicated concentrations. Green fluorescence indicates live bacteria, whereas red fluorescence indicates dead bacteria. Scale bars, 20 μm. F: Quantification of live and dead bacteria based on SYTO-9/PI fluorescence intensities measured using ImageJ. Each dot represents one biological replicate. P values indicate comparisons with the PBS group. G: Development of bacterial resistance during serial passage in the presence of 0.5×MIC of SS-CATH, Polymyxin B, or ciprofloxacin. MICs were determined every five passages. Data are presented as mean±SD from three independent biological replicates. Statistical significance was determined by one-way ANOVA. ns: Not significant; *: $P<0.05$; **: $P<0.01$; ***: $P<0.001$; ****: $P<0.0001$.

uncorrected proof

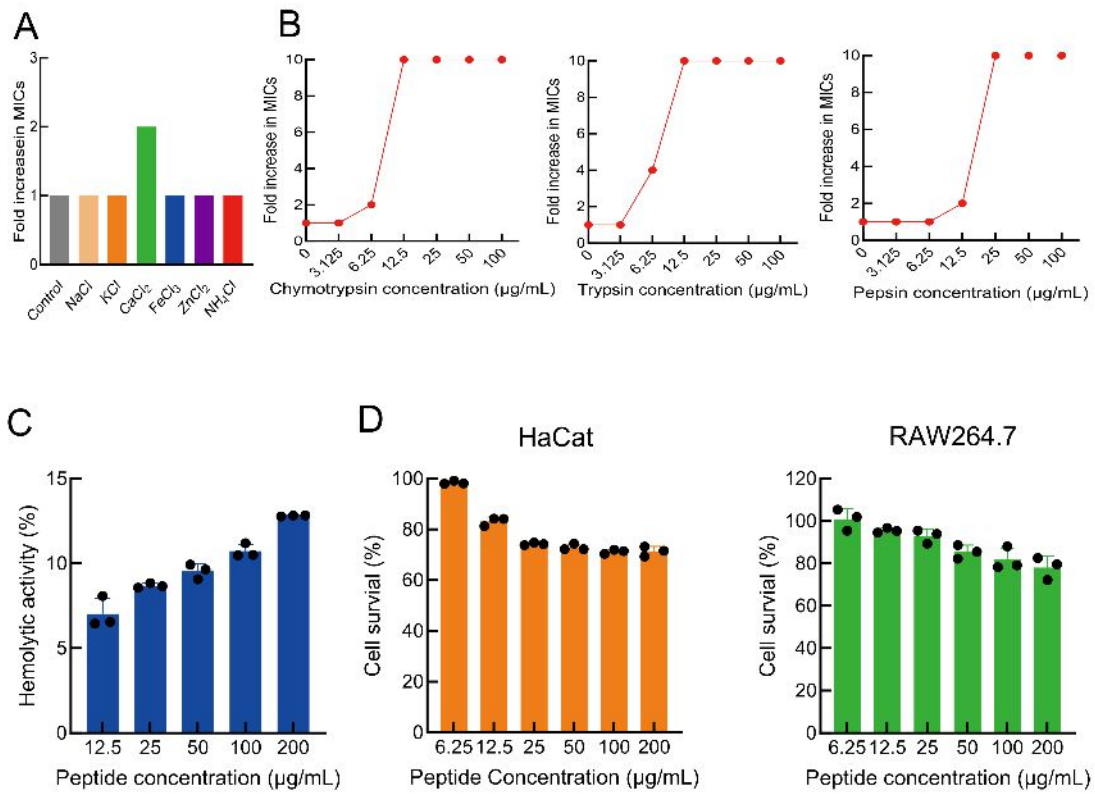


Figure 3. Stability and *in vitro* biocompatibility evaluation of SS-CATH. A: Effect of physiological concentrations of ions (NaCl, KCl, $CaCl_2$, $FeCl_3$, $ZnCl_2$, and NH_4Cl) on the antibacterial activity of SS-CATH, expressed as fold changes in the MIC. B: Effect of 2 h incubation with trypsin, chymotrypsin, or pepsin at 37°C on the antibacterial activity of SS-CATH, expressed as fold increases in MIC relative to the untreated control. C: Hemolytic activity of SS-CATH against mouse erythrocytes at different peptide concentrations. D: Cytotoxicity of SS-CATH toward HaCat keratinocytes and RAW264.7 macrophages determined by the MTT assay after treatment with different concentrations of peptide. All experiments were performed with three independent biological replicates. Data are presented as the mean±SD. Each dot represents one independent biological replicate.

Unconnects

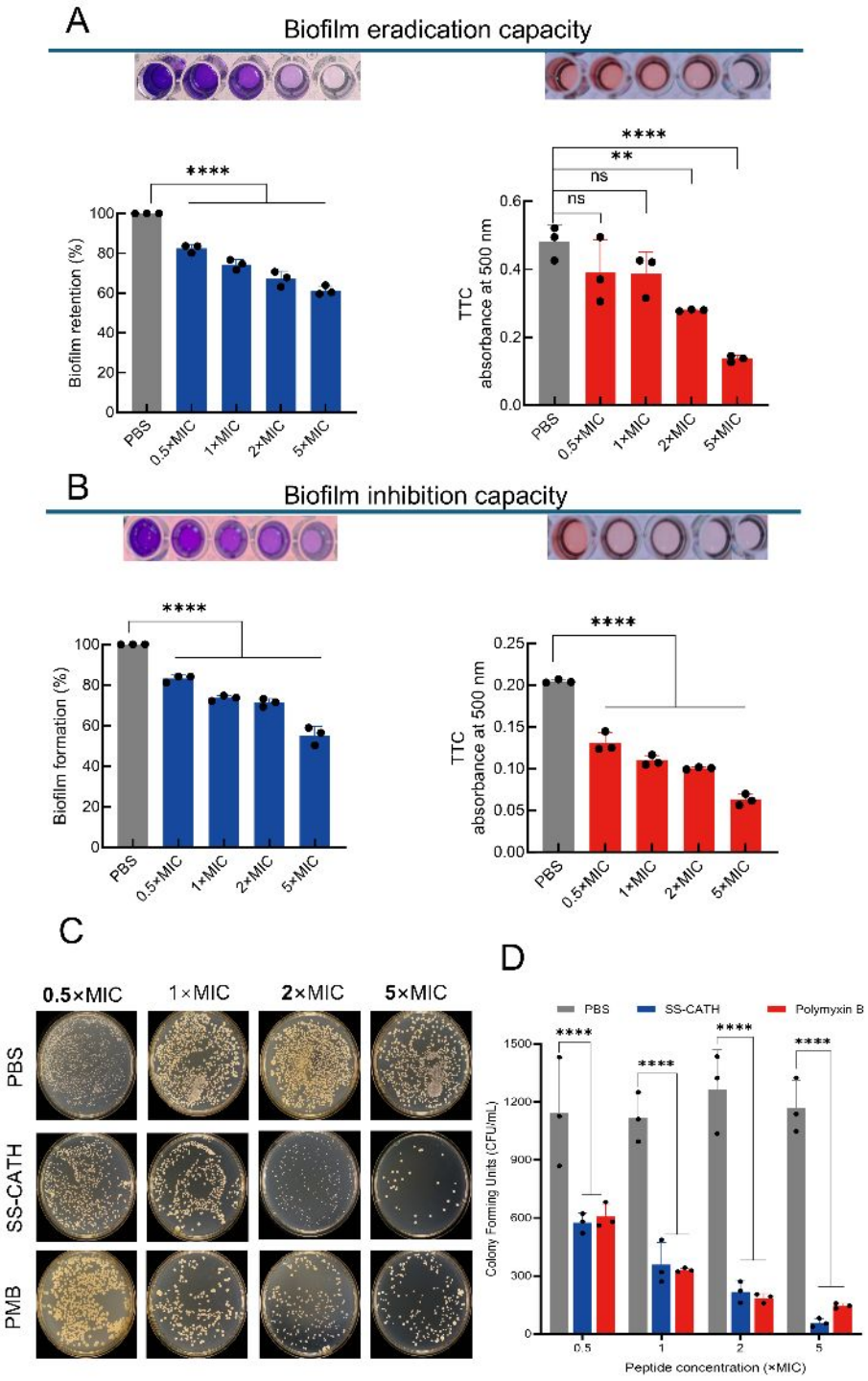


Figure 4. Anti-biofilm and anti-persister activities of SS-CATH. A: Eradication of preformed biofilms by SS-CATH determined by crystal violet staining (left) and 2,3,5-triphenyltetrazolium chloride (TTC) staining (right). B: Inhibition of biofilm formation by SS-CATH determined by crystal violet staining (left) and TTC staining (right). C: Representative

colony images showing the killing of rifampicin-induced persister cells following treatment with SS-CATH or Polymyxin B at different concentrations. PBS served as the negative control. D: Quantification of surviving persister cells by CFU counting. All experiments were performed with three independent biological replicates. Data are presented as the mean±SD. Statistical significance was analyzed using one-way ANOVA, and asterisks indicate the level of significance. Each dot represents one independent biological replicate. ns: Not significant; *: $P<0.05$; **: $P<0.01$; ***: $P<0.001$; ****: $P<0.0001$.

uncorrected proof

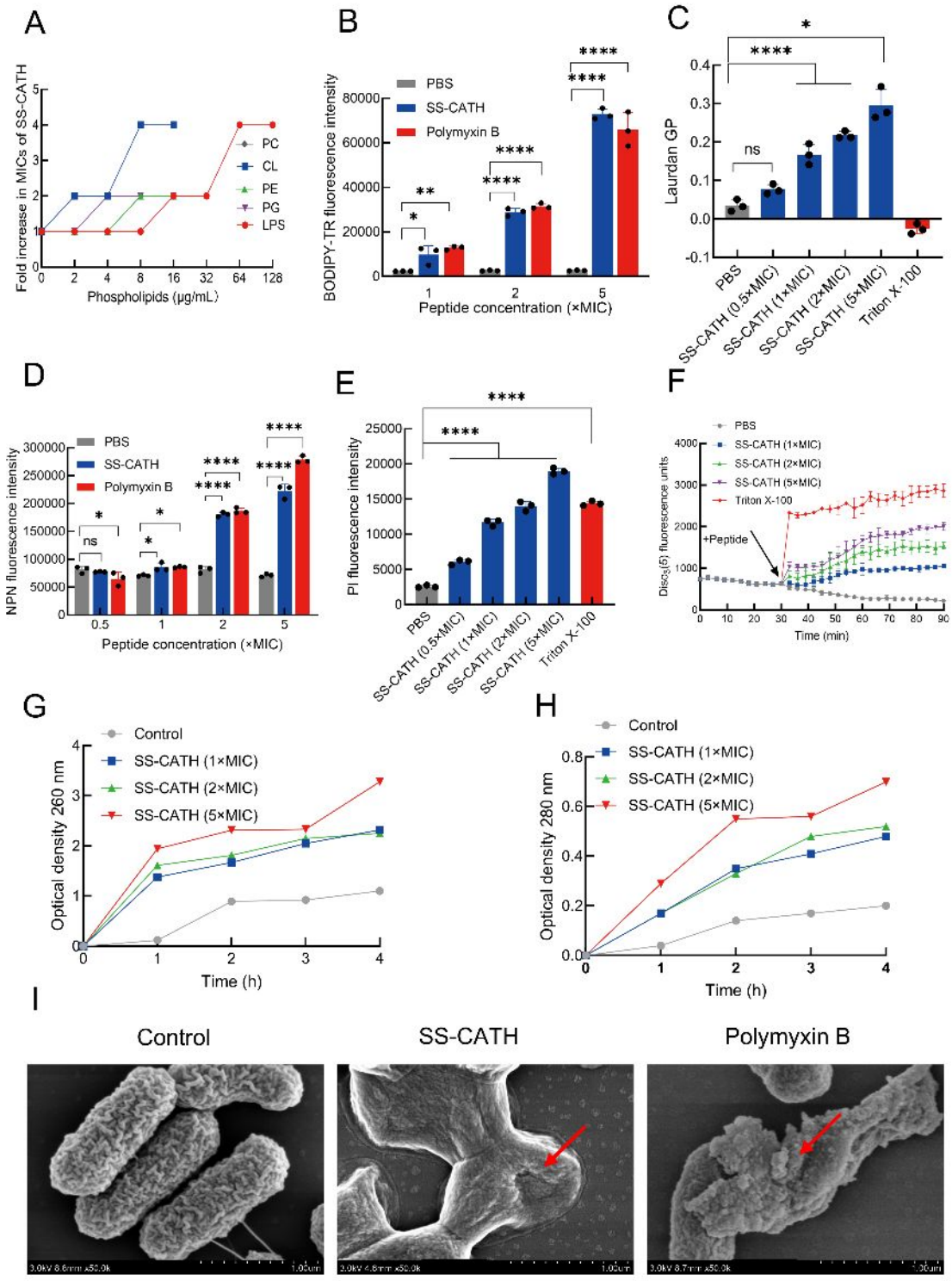


Figure 5. Membrane-targeting mechanism of SS-CATH against Gram-negative bacteria.

A: Phospholipid-binding assay showing the effects of LPS, CL, PE, PG, and PC on the antibacterial activity of SS-CATH, expressed as fold changes in the MIC. B: Binding of SS-CATH to LPS determined by the BODIPY-TR cadaverine displacement assay. C: Changes in

bacterial membrane fluidity following SS-CATH treatment determined by Laurdan fluorescence and expressed as GP values. D: Outer membrane permeabilization induced by SS-CATH determined using the NPN uptake assay. E: Inner membrane permeabilization induced by SS-CATH determined by PI fluorescence. Triton X-100 served as the positive control. F: Membrane depolarization induced by SS-CATH monitored using the $DiSC_3(5)$ fluorescence assay. G, H: Release of intracellular nucleic acids and proteins following SS-CATH treatment, determined by optical density measurements at OD_{260} and OD_{280}, respectively. I: Representative scanning electron microscopy (SEM) images showing the morphological changes of bacterial cells after SS-CATH treatment. Red arrows indicate damaged bacterial cells. Scale bar, 1 μm. All experiments were performed with three independent biological replicates. Data are presented as the mean±SD. Statistical significance was analyzed using one-way ANOVA. ns: Not significant; *: $P<0.05$; **: $P<0.01$; ***: $P<0.001$; ****: $P<0.0001$.

uncorrected proof

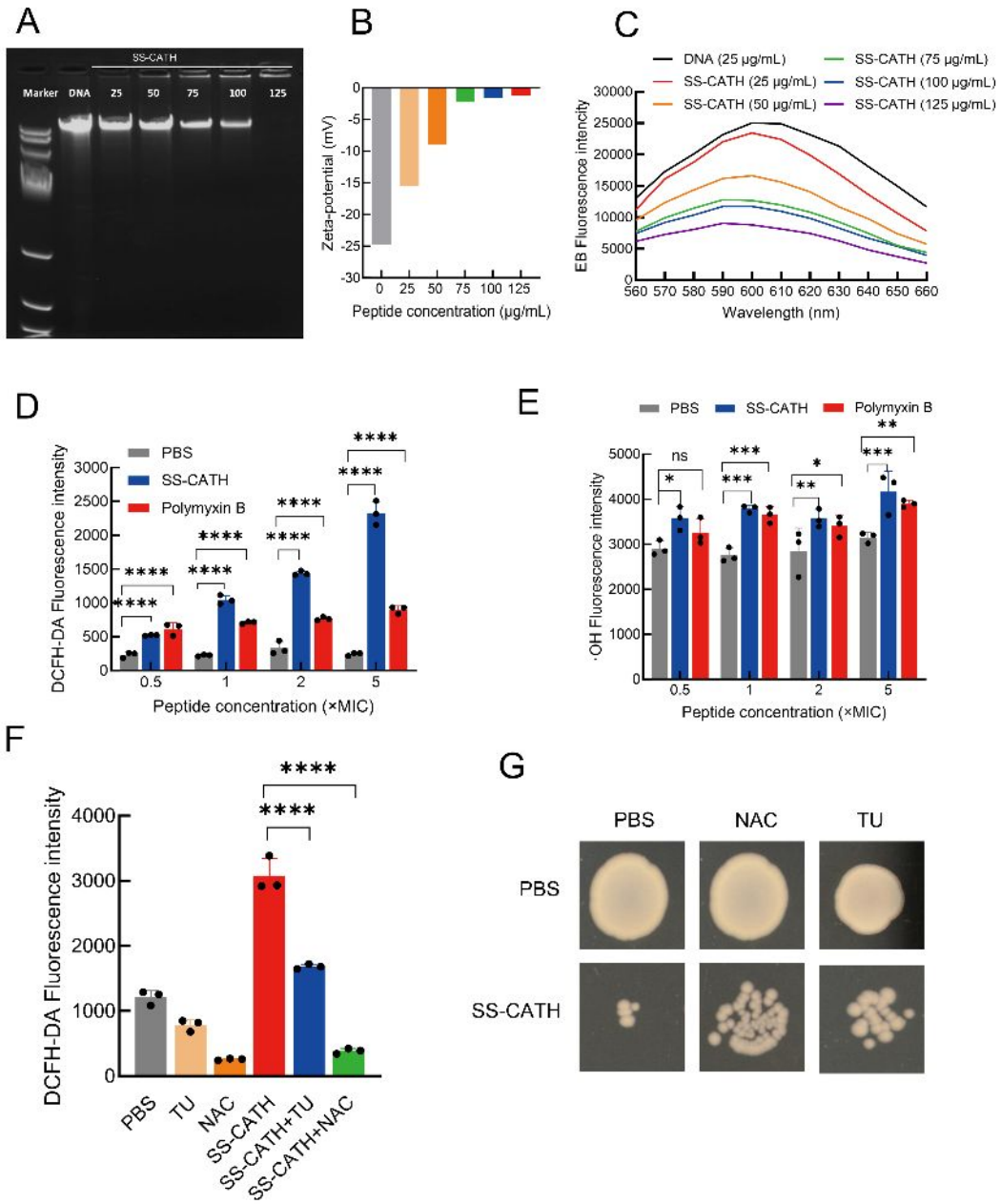


Figure 6. Interaction of SS-CATH with bacterial genomic DNA and induction of oxidative stress. A: Agarose gel retardation assay showing the interaction between SS-CATH and bacterial genomic DNA. B: Zeta potential analysis of bacterial genomic DNA following incubation with different concentrations of SS-CATH. C: EB displacement assay showing the

interaction between SS-CATH and bacterial genomic DNA. D: Intracellular ROS levels induced by SS-CATH, determined using the DCFH-DA fluorescent probe. E: Intracellular •OH production following SS-CATH treatment, determined using the HPF fluorescent probe. F: Intracellular ROS levels following co-treatment with SS-CATH and the ROS scavenger NAC or the hydroxyl radical scavenger TU. G: Representative colony images showing bacterial survival following co-treatment with SS-CATH and NAC or TU. All experiments were performed with three independent biological replicates. Data are presented as the mean±SD. Statistical significance was analyzed using one-way ANOVA. ns: Not significant; *: P<0.05; **: P<0.01; ***: P<0.001; ****: P<0.0001.

uncorrected proof

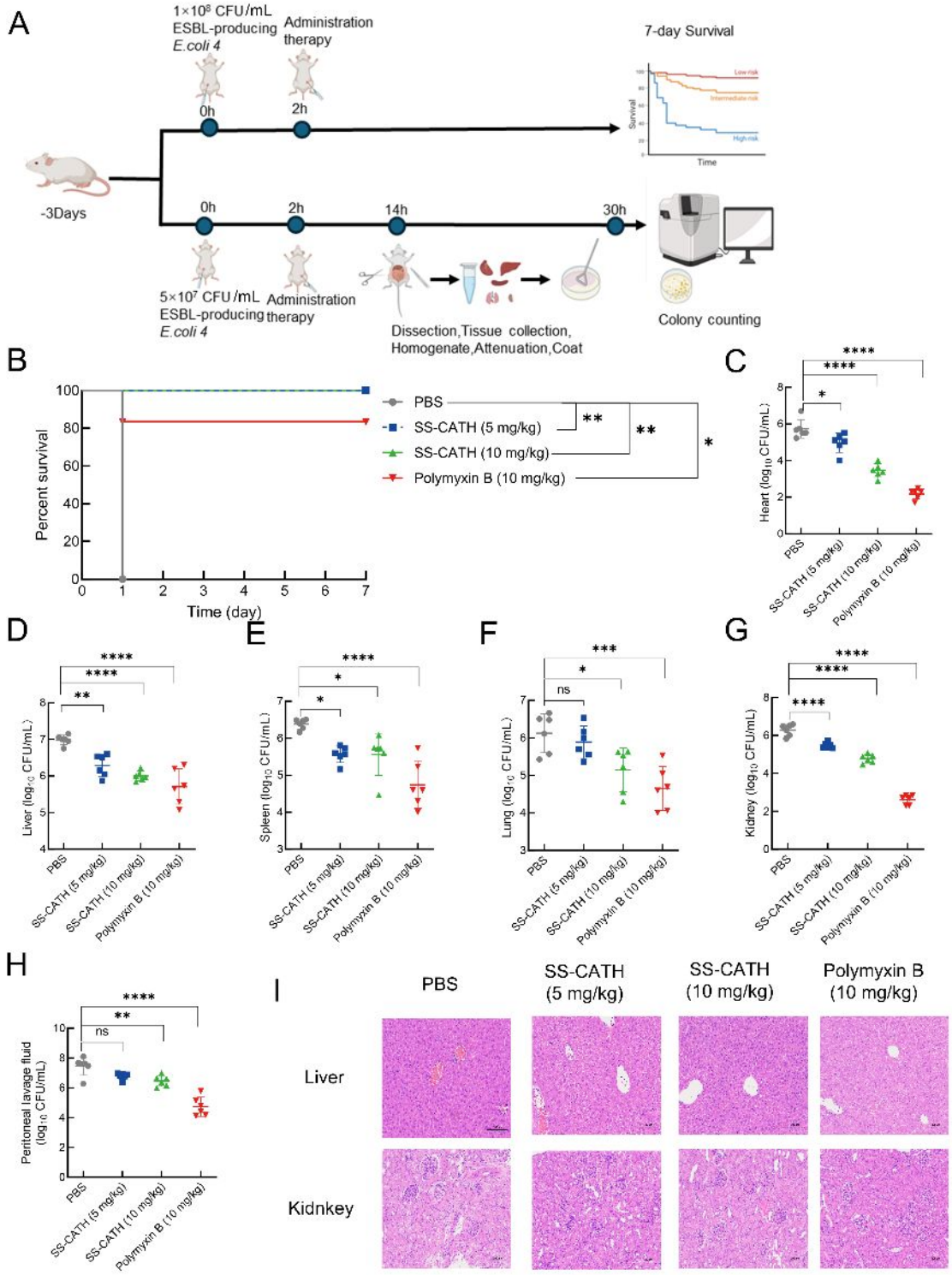


Figure 7. Therapeutic efficacy of SS-CATH in a murine peritonitis model. A: Schematic illustration of the experimental design. Two hours after infection with ESBL-producing *E. coli* 4, BALB/c mice were allocated to groups with comparable mean body weights, and PBS, SS-CATH (5 or 10 mg/kg), or Polymyxin B (10 mg/kg) was randomly assigned to the coded groups

and administered by intraperitoneal injection. Survival was monitored for 7 days. In a parallel experiment, mice were euthanized 12 h after treatment for bacterial burden determination and histopathological analysis. B: Kaplan–Meier survival curves of mice monitored for 7 days following different treatments (n=6 mice per group). Survival curves were compared using the log-rank (Mantel–Cox) test with Bonferroni correction for the three pairwise comparisons against PBS. Adjusted P values are shown. C–H: Bacterial burdens ($\log_{10}$ CFU/mL) in the heart, liver, spleen, lung, kidney, and peritoneal lavage fluid after treatment. I: Representative H&E-stained sections of liver and kidney tissues from each treatment group showing pathological changes. Scale bar, 100 μm**.** For panels C–H, data are presented as mean±SD from independent biological replicates (n=6 mice per group). Statistical significance was analyzed by one-way ANOVA followed by Tukey's post hoc test. ns: Not significant; *: P<0.05; **: P<0.01; ***: P<0.001; ****: P<0.0001.

uncorrected proof

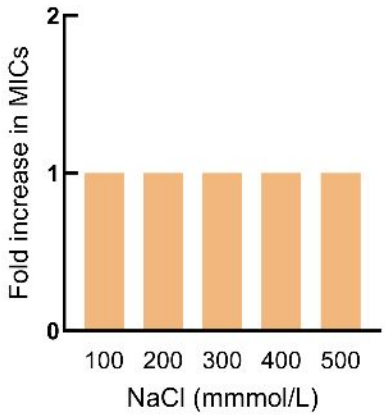
Table 1. Antimicrobial activities of SS-CATH.

Microorganisms	MIC (μmol/L (μg/mL))	
	SS-CATH	Polymyxin B
Gram-negative		
E. coli ATCC25922	0.56 (2.34)	0.84 (1.17)
ESBL-producing *E. coli* 1	8.94 (37.50)	0.84 (1.17)
ESBL-producing *E. coli* 2	4.47 (18.75)	0.84 (1.17)
ESBL-producing *E. coli* 3	2.24 (9.38)	0.84 (1.17)
ESBL-producing *E. coli* 4	2.24 (9.38)	3.36 (4.69)
A. baumannii ATCC19606	2.24 (9.38)	1.69 (2.34)
MDR *A. baumannii* 1	2.24 (9.38)	0.84 (1.17)
MDR *A. baumannii* 2	2.24 (9.38)	0.84 (1.17)
MDR *A. baumannii* 3	1.12 (4.69)	1.69 (2.34)
K. pneumoniae ATCC10031	2.24 (9.38)	0.84 (1.17)
CR *K. pneumoniae* 1	4.47 (18.75)	0.84 (1.17)
CR *K. pneumoniae* 3	2.24 (9.38)	0.84 (1.17)
MDR *P. aeruginosa* 1	2.24 (9.38)	0.84 (1.17)
MDR *P. aeruginosa* 2	2.24 (9.38)	0.84 (1.17)
MDR *P. aeruginosa* 3	2.24 (9.38)	0.84 (1.17)
A. hydrophila	0.56 (2.34)	3.36 (4.69)
E. tarda	0.28 (1.17)	0.84 (1.17)
GM*	1.90 (7.94)	1.07 (1.49)
Gram-positive		
S. aureus CMCC26003	2.24 (9.38)	27.05 (37.50)

Uncorrected proof

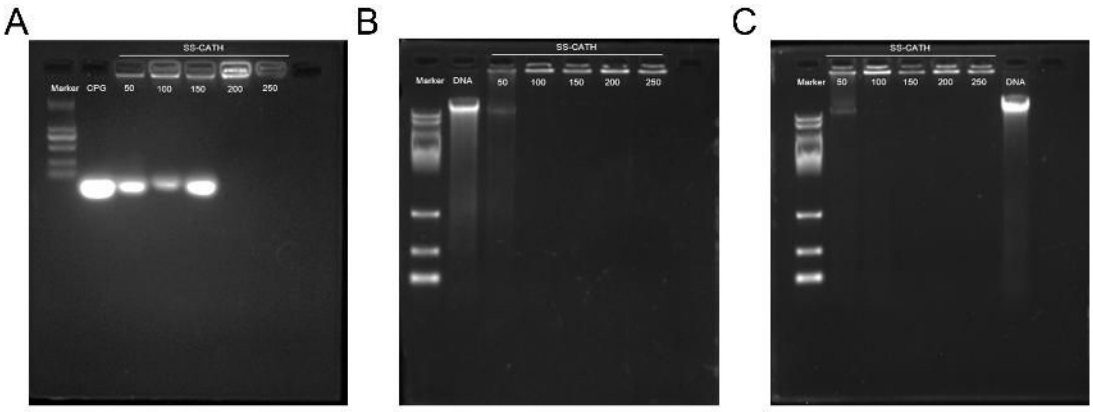
MRSA 52	>24.10 (>100.00)	>72.20 (>100.00)
MRSA USA300	>24.10 (>100.00)	54.10 (75.00)
MDR *S. aureus* 2	>24.10 (>100.00)	>72.20 (>100.00)
MDR *S. aureus* 3	>24.10 (>100.00)	54.10 (75.00)
MDR *S. epidermidis* 1	18.10 (75.00)	54.10 (75.00)
MDR *S. epidermidis* 2	18.10 (75.00)	54.10 (75.00)
MDR *S. epidermidis* 3	2.24 (9.38)	27.05 (37.50)
*B. cereus C*MCC63301	4.47 (18.75)	54.10 (75.00)
GM*	11.06 (46.22)	49.45 (68.50)

MIC: minimal inhibitory concentration. GM: The geometric mean (GM) of the peptide MICs against bacteria was calculated. MIC values >100 μg/mL were treated as 100 μg/mL when calculating the GM; the resulting value is a lower-bound estimate.



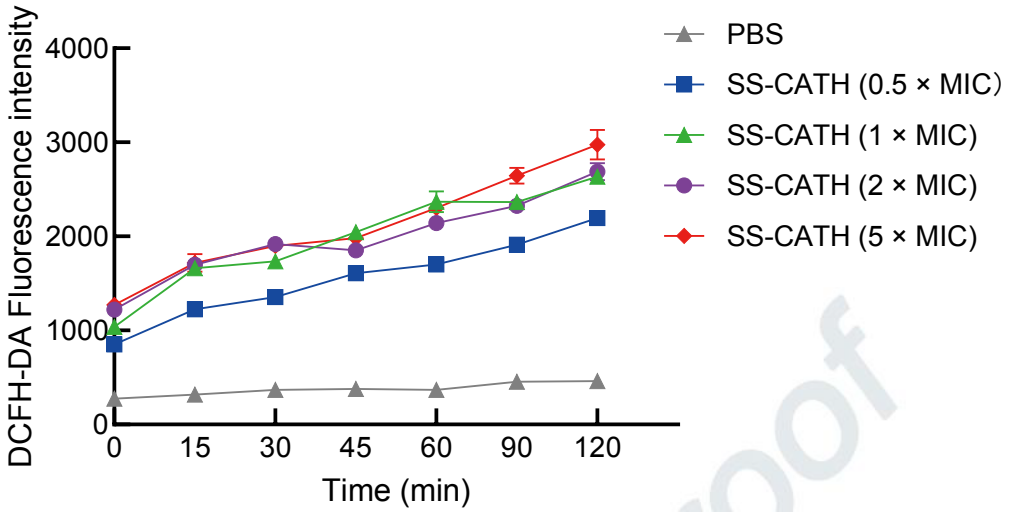
Supplementary Figure S1. Effect of elevated NaCl concentrations on the antibacterial activity of SS-CATH. MICs were determined at final NaCl concentrations of 100, 200, 300, 400, and 500 mmol/L and expressed as fold changes relative to the control without additional NaCl.

uncorrected proof



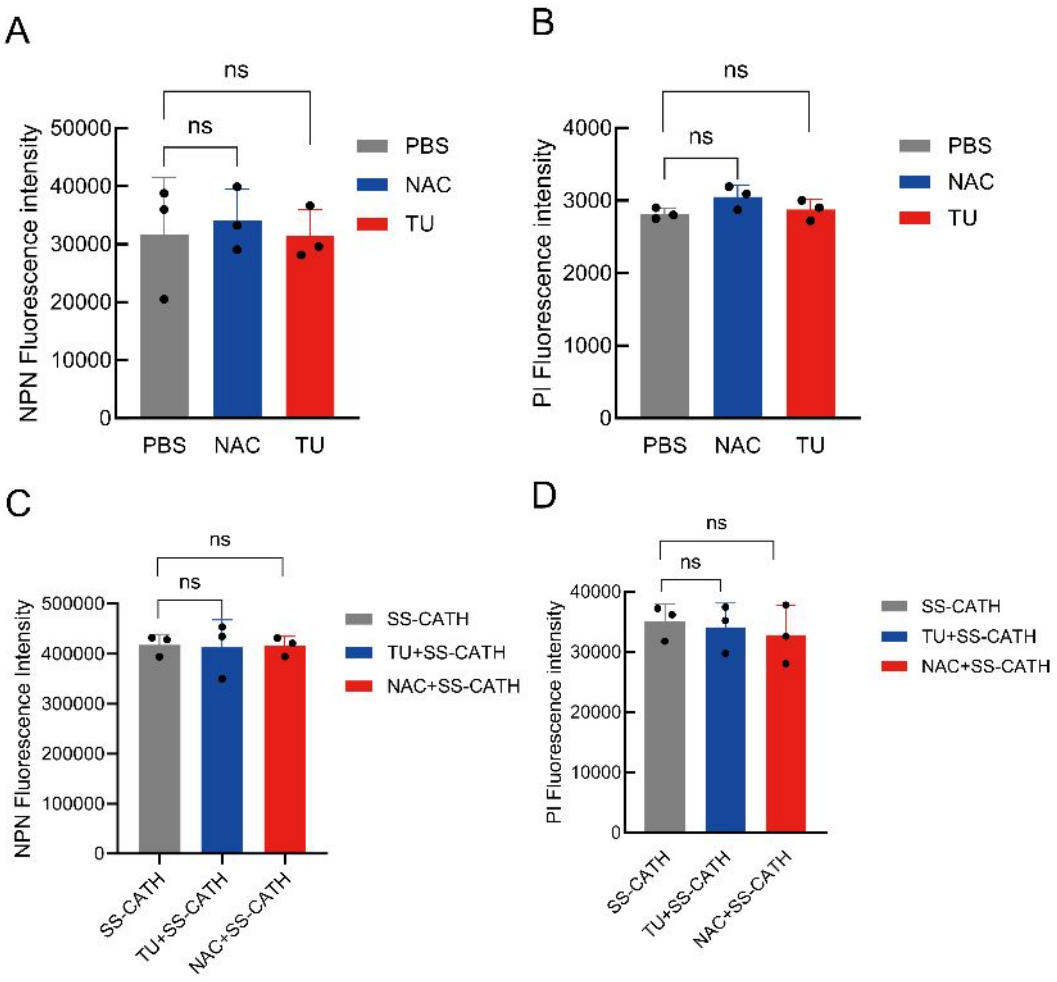
Supplementary Figure S2. Gel retardation assays of SS-CATH with CpG ODN 2395 and mammalian genomic DNA. A: CpG ODN 2395. B: Genomic DNA isolated from RAW264.7 cells. C: Genomic DNA isolated from HaCat cells. Each nucleic acid substrate was maintained at a final concentration of 50 μg/mL and incubated with SS-CATH at final concentrations of 50, 100, 150, 200, and 250 μg/mL, corresponding to nucleic acid-to-peptide mass ratios of 1:1, 1:2, 1:3, 1:4, and 1:5, respectively. The corresponding nucleic acid substrate without SS-CATH served as the control. Numbers above the lanes indicate SS-CATH concentrations in μg/mL. Marker: DL2000 DNA marker in panel A and DL10000 DNA marker in panels B and C.

uncorrected proof



Supplementary Figure S3. Time course of ROS-associated fluorescence following SS-CATH treatment. DCFH-DA fluorescence was measured at the indicated time points in bacteria treated with SS-CATH at 0.5×, 1×, 2×, and 5×MIC. The first measurement was obtained immediately after SS-CATH addition and defined as 0 min. PBS served as the control. Data are presented as mean±SD from three independent biological replicates.

uncorrected proof



Supplementary Figure S4. Effects of NAC and TU on bacterial membrane permeability in the absence and presence of SS-CATH. A, B: NPN and PI fluorescence, respectively, in bacteria treated with PBS, NAC, or TU in the absence of SS-CATH. C, D: NPN and PI fluorescence, respectively, in bacteria treated with SS-CATH alone or in combination with NAC or TU. Data are presented as mean±SD from three independent biological replicates (n=3). Each dot represents one independent biological replicate. Statistical significance was analyzed using one-way ANOVA followed by Tukey's post hoc test. P values indicate comparisons with PBS in panels A and B and with SS-CATH alone in panels C and D. ns: Not significant; *: P<0.05; **: P<0.01; ***: P<0.001; ****: P<0.0001.

Uncorrected

中文摘要：

海蛇保守型抗菌肽 SS-CATH 的鉴定及其对多重耐药革兰氏阴性菌的功能表征

作者：徐美琳[1,4]，李双宇[1,4]，徐志康[2]，刘至臻[1,3]，宋一晓[1,4]，张晶晶[1,4]，孔祥金[1,4]，宋鹏[5,6*]，王义鹏[1,4*]

[1]中国科学院烟台海岸带研究所，山东烟台 264003

[2]江苏省长江中下游生物多样性保护与可持续利用重点实验室，南京师范大学生命科学学院，江苏南京 210000

[3]济南大学生物科学与技术学院，山东济南 250022

[4]中国科学院大学，北京 100049

[5] 聊城大学药学与食品工程学院，山东聊城 252000

[6] 大分子药物与规模化制备全国重点实验室，山东聊城 252000

摘要：海蛇是高度适应海洋环境的爬行动物，长期生活于高盐度等特殊环境中，也可能面临潜在致病性革兰氏阴性菌的感染压力。Cathelicidin 家族抗菌肽（antimicrobial peptides, AMPs）是脊椎动物先天免疫系统的重要组成部分，其成熟肽序列通常在不同物种间具有较高的多样性。本研究通过对多种海蛇基因组进行挖掘和序列分析，发现了一种成熟肽序列高度保守的 Cathelicidin 家族抗菌肽，并将其命名为 SS-CATH。该抗菌肽存在于青环海蛇（*Hydrophis cyanocinctus*）、大海蛇（*Hydrophis major*）、优雅海蛇（*Hydrophis elegans*）和淡灰海蛇（*Hydrophis ornatus*）中。功能研究表明，SS-CATH 对多种多重耐药革兰氏阴性致病菌具有较强的广谱杀菌活性，同时能够抑制细菌生物被膜形成、破坏已形成的生物被膜，并杀灭利福平诱导的持留菌。机制研究发现，SS-CATH 能够破坏细菌细胞膜完整性并诱导氧化应激，同时在体外表现出 DNA 结合活性。在小鼠腹膜炎感染模型中，SS-CATH 显著提高了感染小鼠的生存率，并降低了多个器官中

uncorrected proof

的细菌负荷。SS-CATH 在不同海蛇物种间表现出的序列保守性提示其可能受到功能约束，而其抗菌活性也表明该肽可能参与宿主防御。本研究发现了一种在多种海蛇中高度保守的抗菌肽，并对其功能进行了初步分析。这一发现有助于进一步认识海蛇先天免疫系统的适应性特征，也为开发针对多重耐药革兰氏阴性菌感染的新型抗菌候选分子提供了研究基础

关键词：海蛇；Cathelicidin 家族抗菌肽；抗菌肽；多重耐药菌；革兰氏阴性菌；抗菌机制；先天免疫

通讯作者：宋鹏（songpeng@lcu.edu.cn）；王义鹏（ypwang@yic.ac.cn）

uncorrected proof